

387496

Report 2304

AD 655249

THE INELASTIC BUCKLING STRENGTH OF FABRICATED HY-80 STEEL HEMISPHERICAL SHELLS

NAVAL SHIP RESEARCH AND DEVELOPMENT CENTER



THE INELASTIC BUCKLING STRENGTH OF  
FABRICATED HY-80 STEEL HEMISPHERICAL SHELLS

by

M.G. Costello and K. Nishida

Distribution of this document is unlimited

STRUCTURAL MECHANICS LABORATORY  
RESEARCH AND DEVELOPMENT REPORT

RECEIVED

AUG 1 1967

CFSTI

April 1967



Report 2304

THE INELASTIC BUCKLING STRENGTH OF  
FABRICATED HY-80 STEEL HEMISPHERICAL SHELLS

by

M.G. Costello and K. Nishida

Distribution of this document is unlimited

April 1967

Report 2304  
S-F013 01 03, Task 0214  
S-F013 03 02, Task 1960

## TABLE OF CONTENTS

	Page
ABSTRACT .....	1
ADMINISTRATIVE INFORMATION .....	1
INTRODUCTION .....	1
DESCRIPTION OF MODELS .....	2
PROCEDURE .....	3
DETERMINATION OF INITIAL IMPERFECTIONS .....	3
TEST PROCEDURE .....	17
RESULTS AND DISCUSSION .....	27
CONCLUSIONS .....	37
ACKNOWLEDGMENTS .....	39
REFERENCES .....	40

## LIST OF FIGURES

	Page
Figure 1 - Model and Cylinder Assembly .....	4
Figure 2 - Typical Stress-Strain Plots for Model 82 from Original Plate and Model after Hydrostatic Testing .....	6
Figure 3 - Distribution of Yield Strength from a Typical Formed Segment of Model 82 after Test .....	7
Figure 4 - Deviations from Sphericity .....	8
Figure 5 - Arc Length Scales .....	16
Figure 6 - Strain-Gage Locations and Strain Sensitivities .....	22
Figure 7 - Test Setup .....	26
Figure 8 - Typical Pressure-Strain Plots .....	28
Figure 9 - Models after Collapse .....	32
Figure 10 - Nondimensional Plot of Experimental Results for Fabricated HY-80 Steel Spherical Shells .....	35

# LIST OF TABLES

	Page
Table 1 - Compressive Yield Strengths .....	5
Table 2 - Measured Wall Thickness of the Models .....	18
Table 3 - Local Geometry and Comparison of Calculated and Measured Membrane Stresses and Collapse Pressures .....	38

## ABSTRACT

Eight, 66-in.-diameter, fabricated HY-80 steel hemispherical shells designed to fail by inelastic buckling were tested to observe the effects of initial imperfections and residual stresses on elastic behavior and collapse strength. The results demonstrate that the effect of secondary moments and residual stresses on collapse strength diminish as the ratio of elastic to inelastic buckling pressure increases. It was possible to predict the collapse pressures of these models within +10 percent by utilizing imperfection analysis and extrapolating previous test results of less stable shells. Fairly good agreement was also obtained by using the same imperfection analysis to predict the membrane stresses in the center of the flat spots. Addition of the results of these tests to those obtained on shells in the less stable regions provides a basis for a reasonable collapse equation for practical spherical shells over the range of shell stability of interest to deep submergence.

## ADMINISTRATIVE INFORMATION

The work described in this report was conducted under the sponsorship of the Special Projects Office, Subproject S-F013 01 03, Task 0214, and the Naval Ships Systems Command, Subproject S-F013 03 02, Task 1960.

## INTRODUCTION

The lack of adequate criteria for designing fabricated spherical shells under hydrostatic loading has been a problem to designers for many years. It is well known that under such loading the elastic buckling strength is considerably less than predicted by classical linear theory. The lower strength is generally attributed to the effects of initial imperfections, residual stresses, and adverse boundary conditions which the theory neglects. Thus, in the absence of adequate criteria, designers have had to resort to high factors of safety and to accept the associated weight penalties.

Interest in deeper diving submarines and small research vehicles has emphasized the need for more adequate criteria. In the past few years, the David Taylor Model Basin has conducted extensive studies of machined

shells to develop the necessary background.<sup>1-4</sup> These led to development of an analysis for near-perfect and initially imperfect, stress-free spherical shells.<sup>5</sup> The investigations were subsequently extended to realistic, large-scale fabricated shells in a parametric study of the buckling strength of HY-80 steel hemispheres.<sup>6</sup> On the basis of these tests, a collapse equation for fabricated shells was proposed, by which collapse strength would be calculated on the basis of measured local imperfection geometry. In the course of this study, it became evident that further tests of more stable shells were required. Thus, eight additional models were designed to investigate the behavior of spherical shells possessing a ratio of elastic-to-inelastic collapse strength of about 2.5 to 4.0. This report discusses the fabrication, test procedures, and results for these eight models.

#### DESCRIPTION OF MODELS

The eight, 66-in.-diameter, hemispherical shell models were fabricated by the Lukens Steel Company from HY-80 steel (nominal yield strength of 80,000 psi). Each model consisted of seven pressed and welded segments; six, 60-deg, orange-peel segments and a 60-deg polar cap. Four of the models (Models 75, 76, 79, and 80) had a nominal thickness to radius  $h/R$  ratio of 0.024 and the other four (Models 77, 78, 81, and 82) had an  $h/R$  ratio of 0.030. Models 76, 80, 78, and 82 were tested in the as-fabricated condition; Models 75, 79, 77, and 81 were tested after stress relieving. In stress relieving the model, the furnace was preheated to a temperature of 1025 F. The model was then inserted in the furnace and stress relieved for 1 hour, after which the model was removed from the furnace and air cooled.

An internally ring-stiffened cylinder was welded to each model prior to testing. Because of the tolerances involved in fabricating spherical shells of this size and the need to employ nominal dimensions in design, it was not practical to utilize cylinders that would ensure membrane

---

<sup>1</sup>References are listed on page 40.

boundaries at the juncture of hemisphere and cylinder. Thus, each plating of the cylinder shell was arbitrarily increased in thickness by approximately 10 percent over that which would provide membrane conditions. Figure 1 shows a model and cylinder assembly and presents nominal model dimensions.

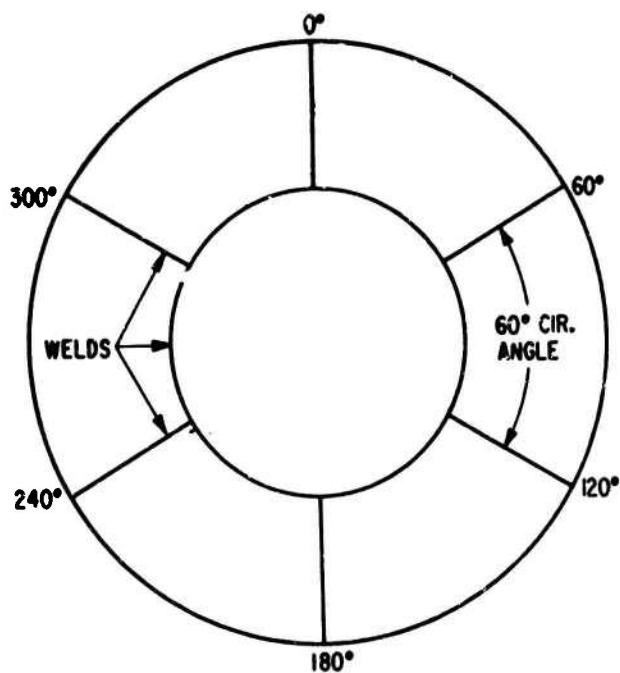
In all calculations, Young's modulus  $E$  and Poisson's ratio  $\nu$  were assumed to be  $30 \times 10^6$  psi and 0.3, respectively. Yield strengths as determined from uniaxial compression tests of the original plate material are presented in Table 1. For the stress-relieved models, the coupons cut from the original plate were stress-relieved along with the models. In all tests, the specimens were 1/2 in. in diameter by 2 in. in length. A typical stress-strain curve of the original plate material of Model 82 (not stress relieved) is presented in Figure 2. In addition to these tests, samplings of yield strength were taken from Model 82 after the hydrostatic test to observe the effect of forming on strength. Locations of specimens and results are presented in Figure 3. Typical stress-strain curves from three different areas of the segment are presented in Figure 2.

## PROCEDURE

### DETERMINATION OF INITIAL IMPERFECTIONS

The analysis<sup>5</sup> for initially imperfect, stress-free spherical shells requires the accurate determination of initial imperfections over the entire surface of the shell. It was therefore necessary to take approximately 1000 radius measurements on each model from a fixed point within the shell to the inside surface. The results of these measurements are presented in the form of contour maps (Figure 4) that represent the inside view of a hemisphere unfolded into a flat surface whose radial scale remains constant. This scale can be determined by dividing one-half the circumference of the sphere by the diameter of the contour map. As in the case with the problem of mapping, the scale in all other directions varies, depending on the distance from the center of the plot and the orientation with the radial direction. To overcome this problem, arc-length scales were utilized together with the contour maps for out-of-roundness analysis. A typical arc-length scale is presented in Figure 5.

(Text continued on page 17.)



Dimension	Models 75,* 76 79,* 80	Models 77,* 78 81,* 82
a	3 1/4	3 3/8
b	1 1/4	1 3/8
c	1 1/8	1 5/16
d	16 3/4	17 5/8
e	1 1/8	1 5/16
f	2 1/2	2 3/4
g	64 5/8	64 9/16
h <sub>s</sub>	13/16	1
j	3 3/4	4 1/8
k	58 1/2	57 3/4

\*Stress Relieved

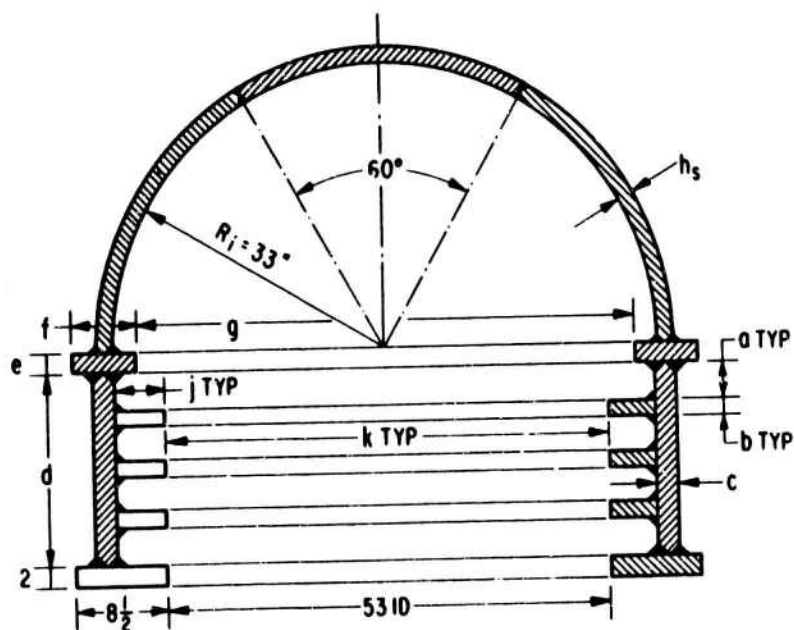


Figure 1 - Model and Cylinder Assembly



TABLE 1  
Compressive Yield Strengths

Model	Yield Strength* Pounds per Square Inch
75**	87,500
79**	87,500
76	87,600
80	87,600
77**	87,700
81*	87,700
78	92,700
82	92,700
<p>* Yield strengths for stress-relieved models determined from specimens which were stress relieved with model.</p> <p>** Indicates stress-relieved models.</p>	

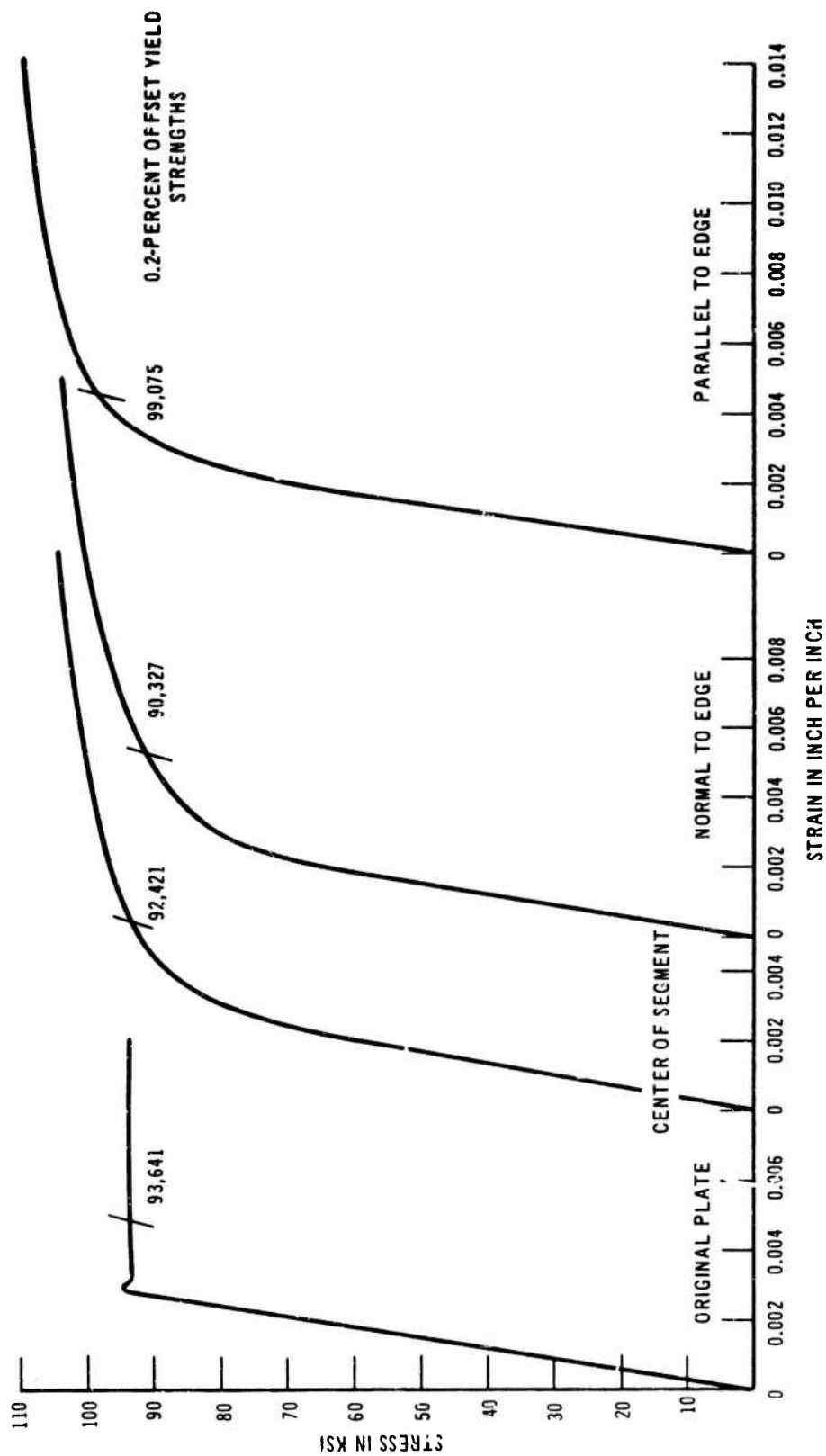
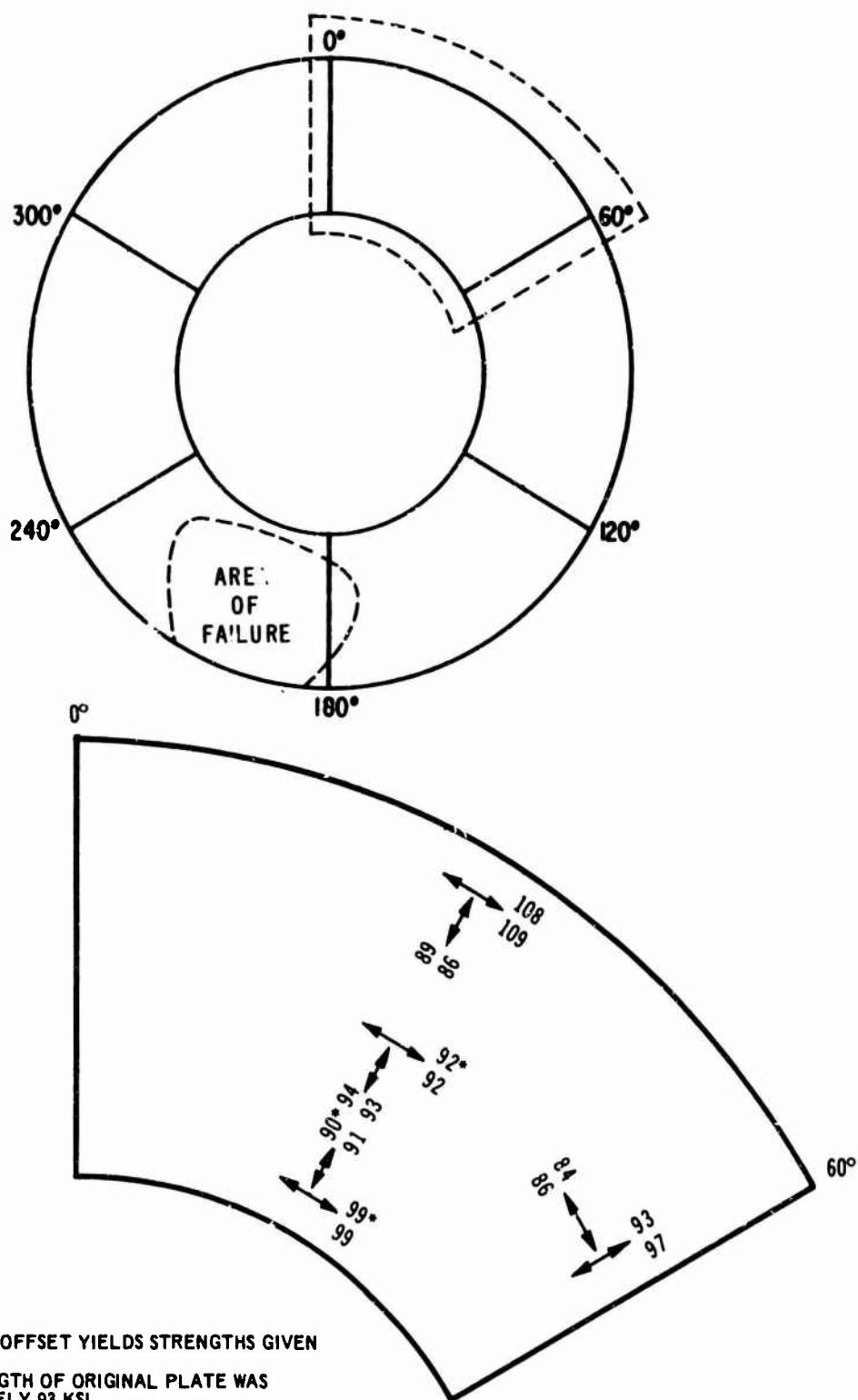


Figure 2 - Typical Stress-Strain Plots for Model 82 from Original Plate and Model after Hydrostatic Testing



NOTES:

1. 0.2 PERCENT OFFSET YIELDS STRENGTHS GIVEN IN KSI.
2. YIELD STRENGTH OF ORIGINAL PLATE WAS APPROXIMATELY 93 KSI.

\*PLOTTED IN FIGURE 9.

Figure 3 - Distribution of Yield Strength from a Typical Formed Segment of Model 82 after Test

Figure 4 - Deviations from Sphericity

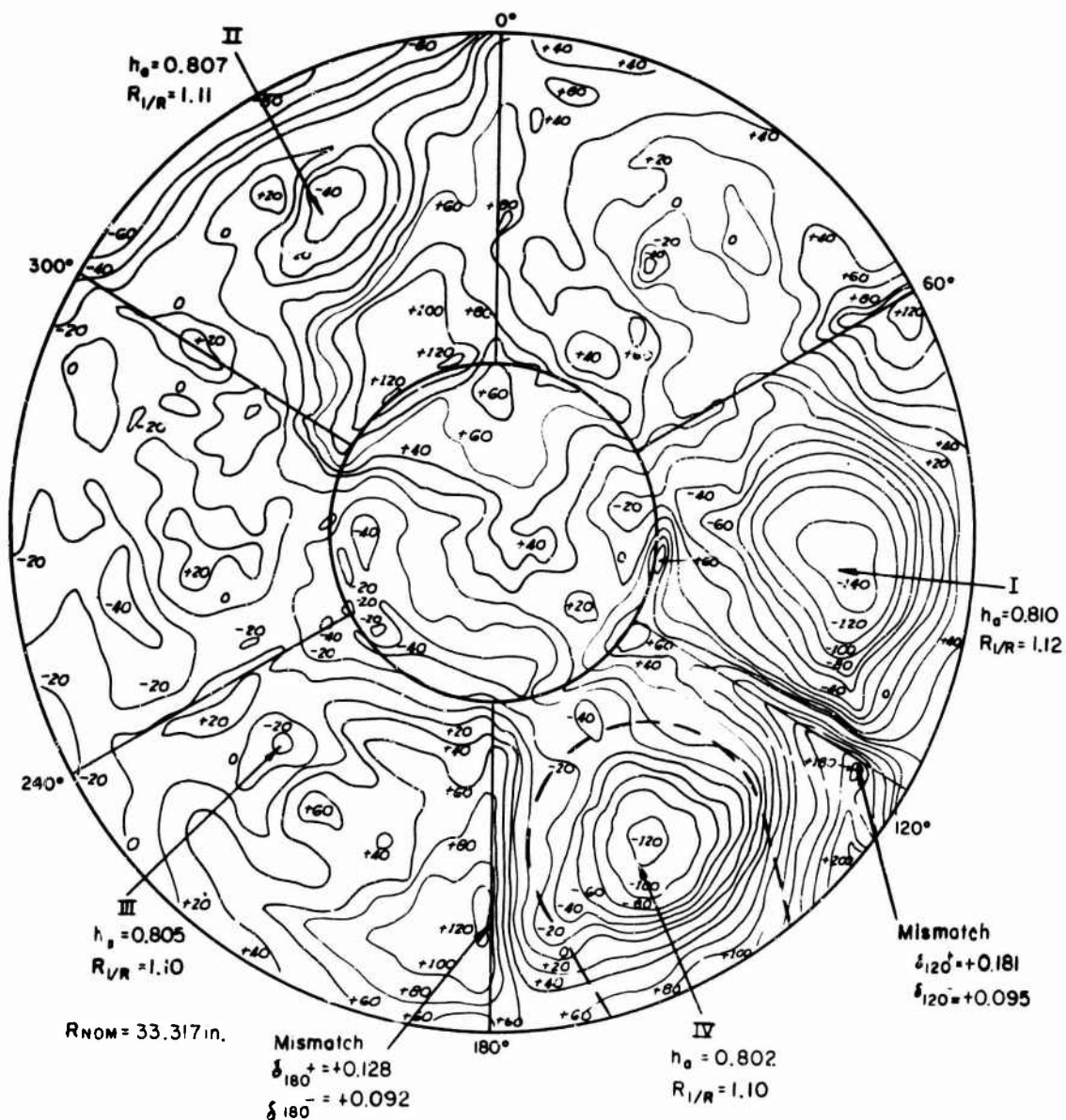


Figure 4a - Model 75

The surface enclosed by the solid circle represents a hemisphere unfolded into a flat surface whose radial scale remains constant. Contours are plotted in mils. Minus contours indicate inward deviations, e.g., -10 indicates distance from center of sphere is  $R_{nom} - 0.010$  in.

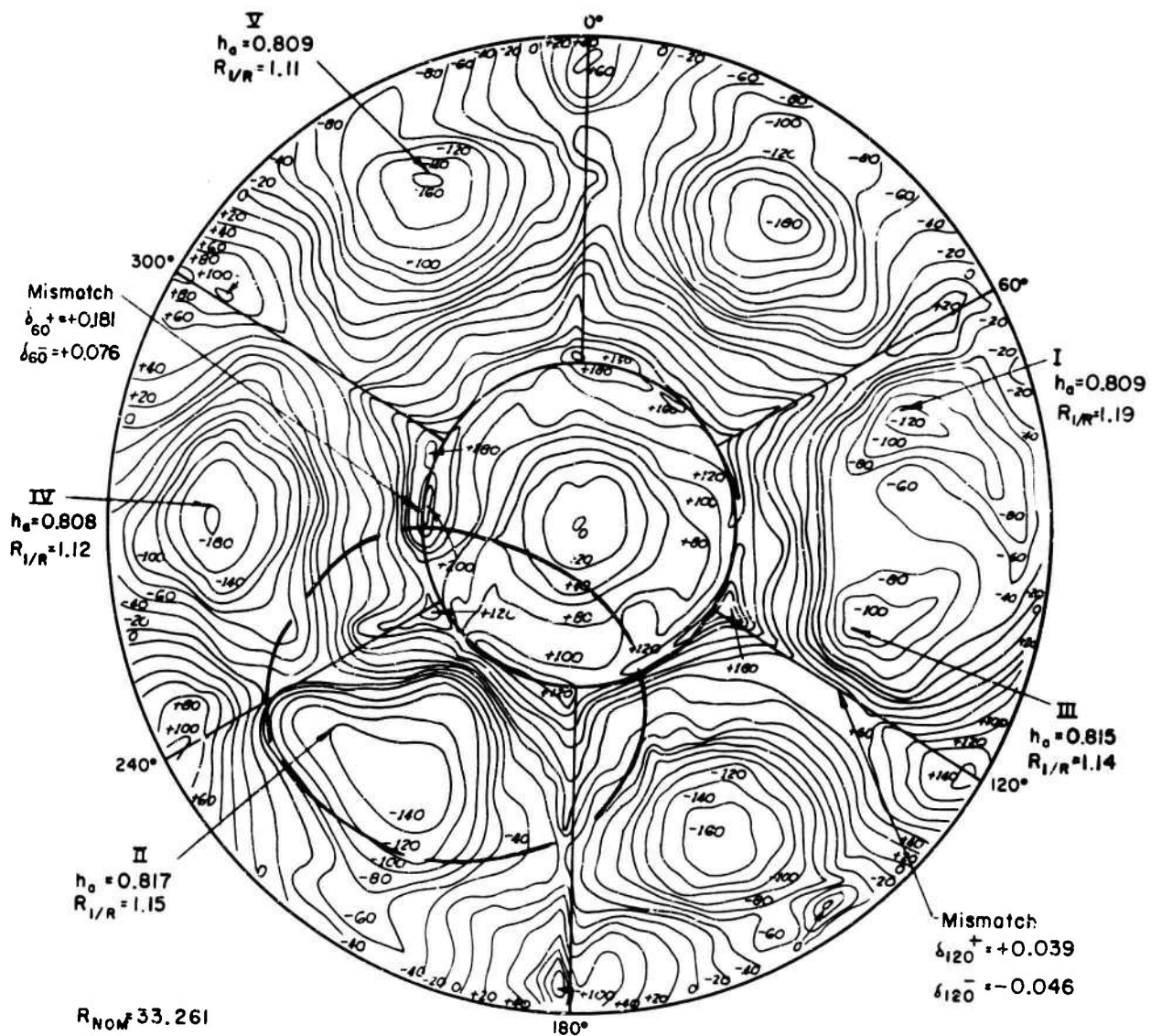


Figure 4b - Model 79

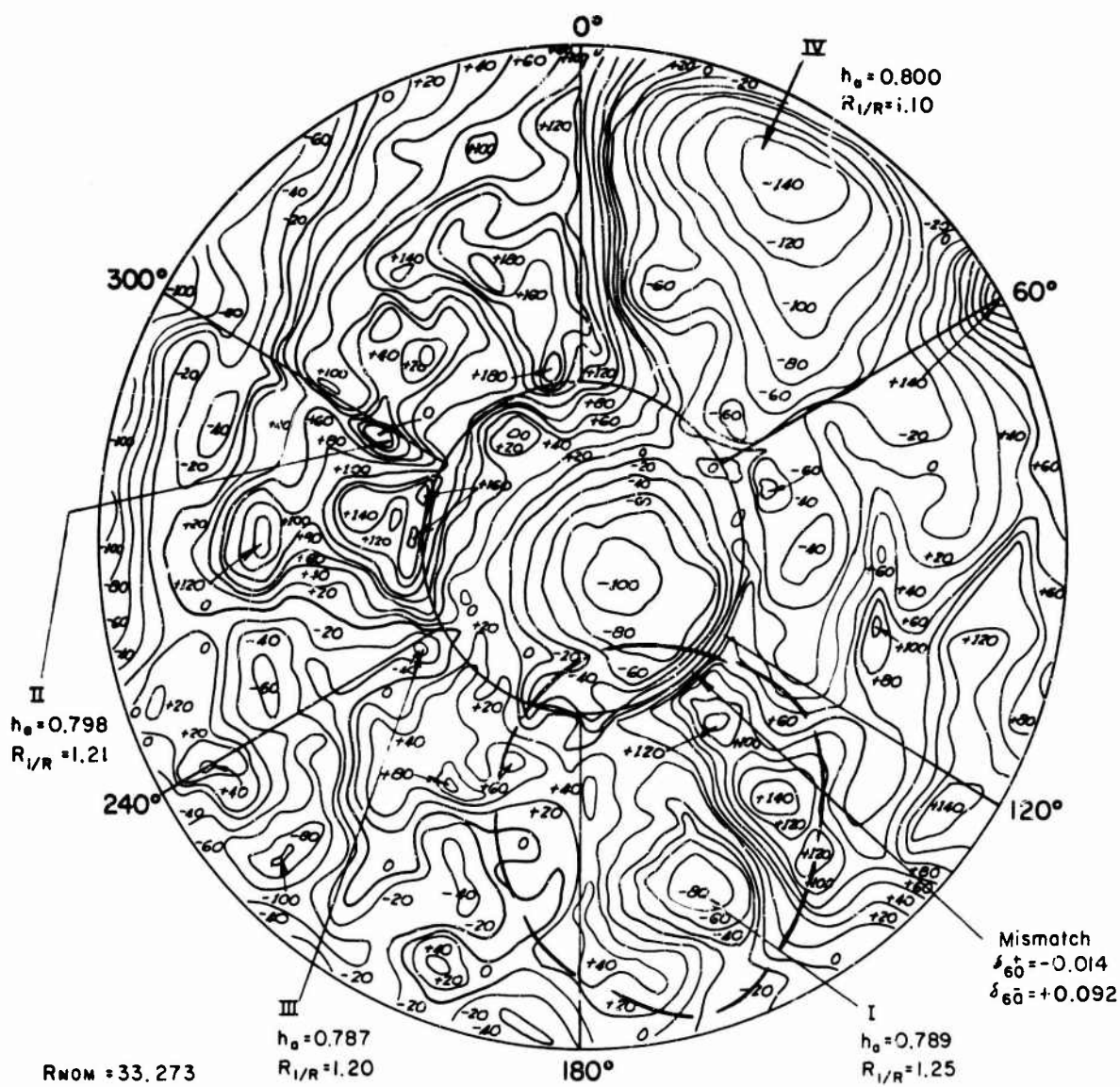


Figure 4c - Model 76

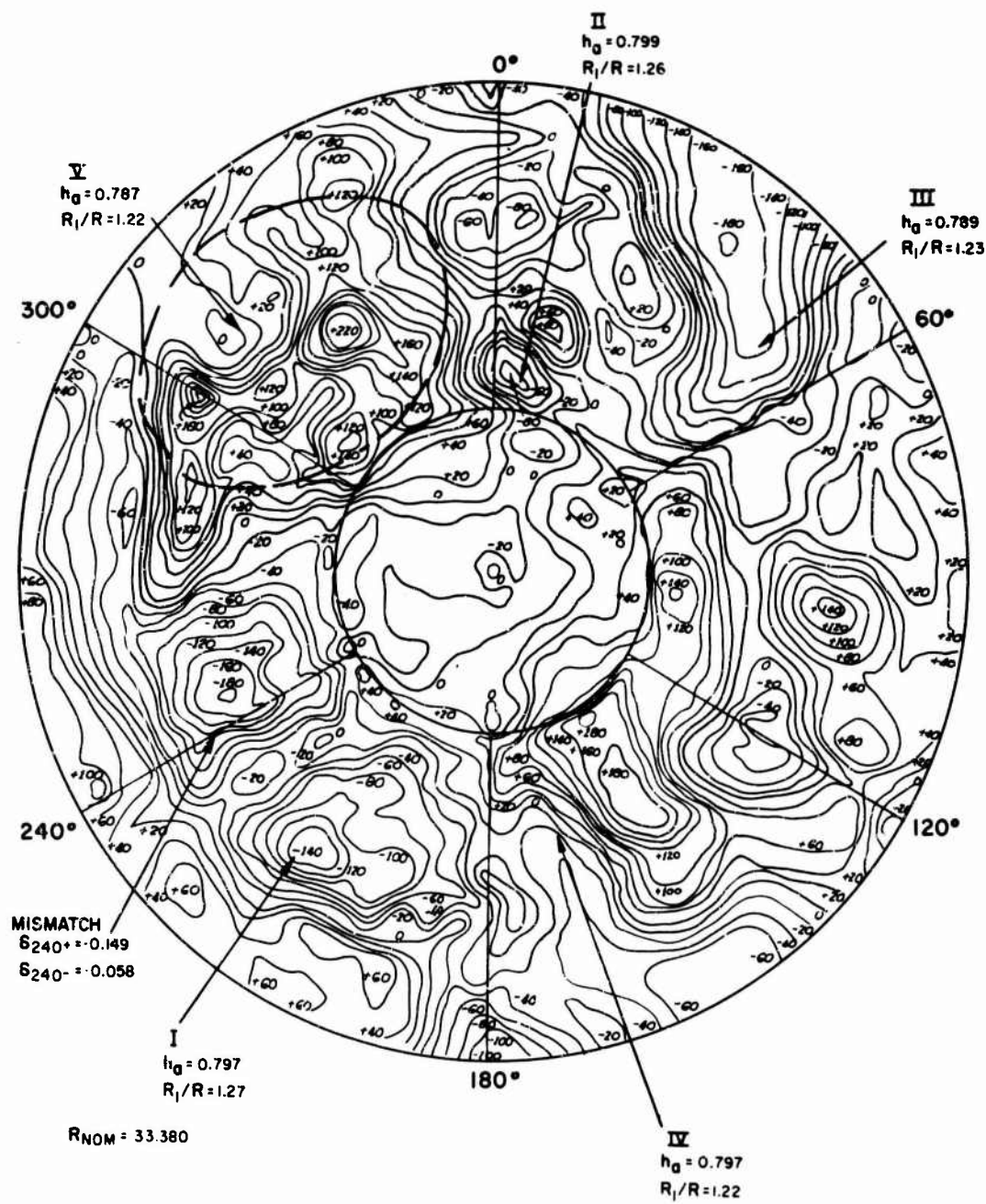


Figure 4d - Model 80



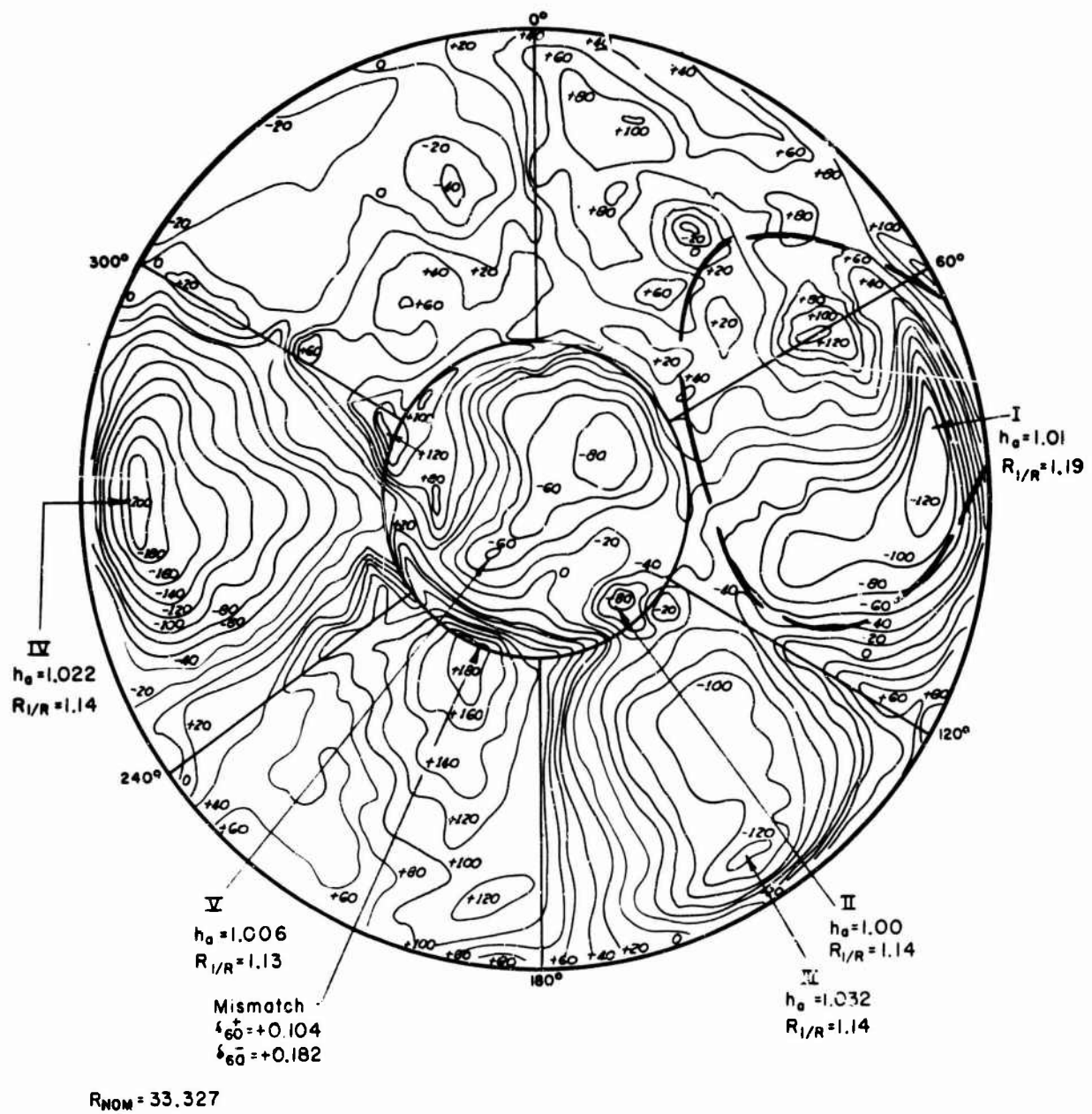


Figure 4e - Model 77



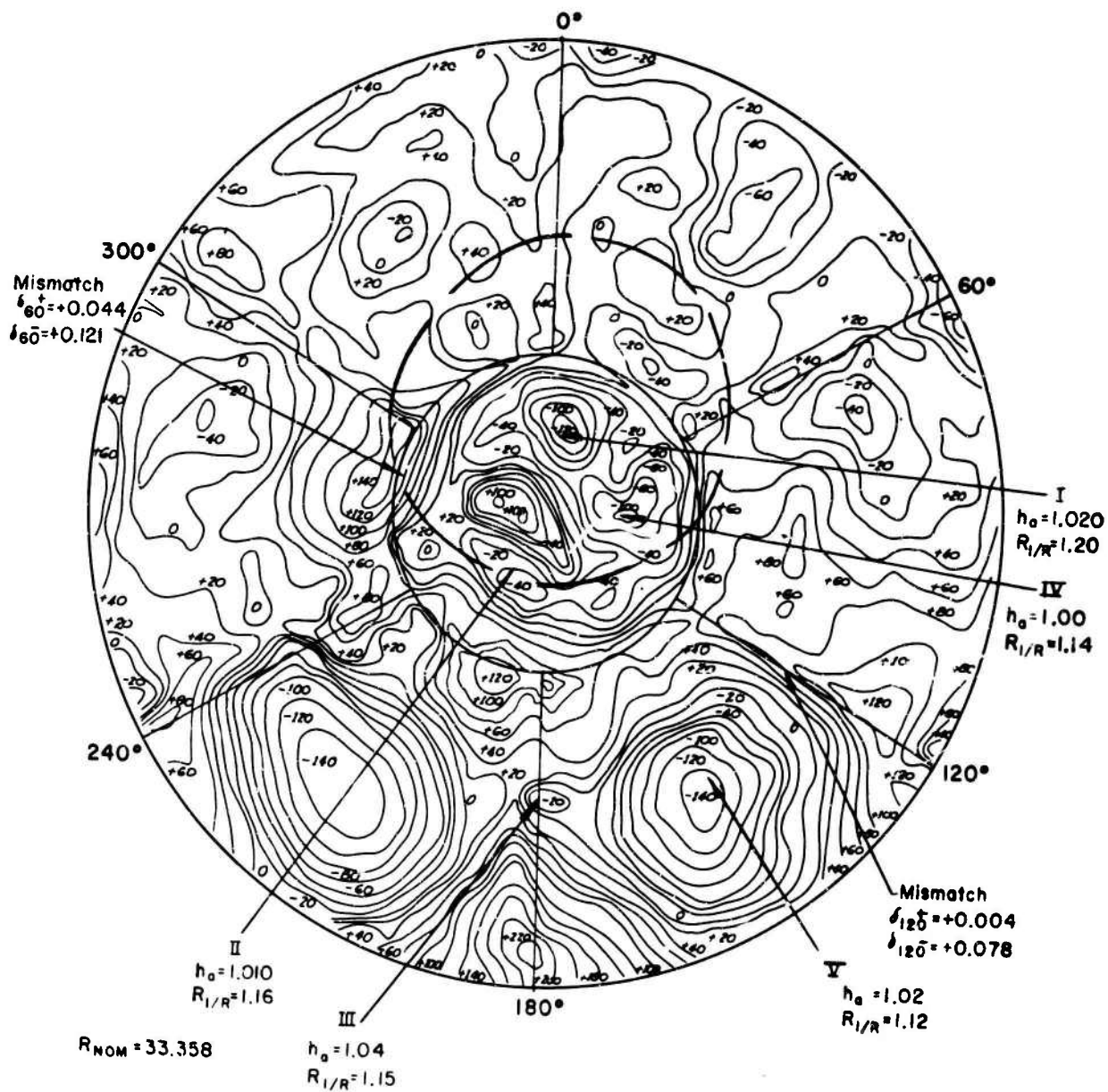


Figure 4f - Model 81

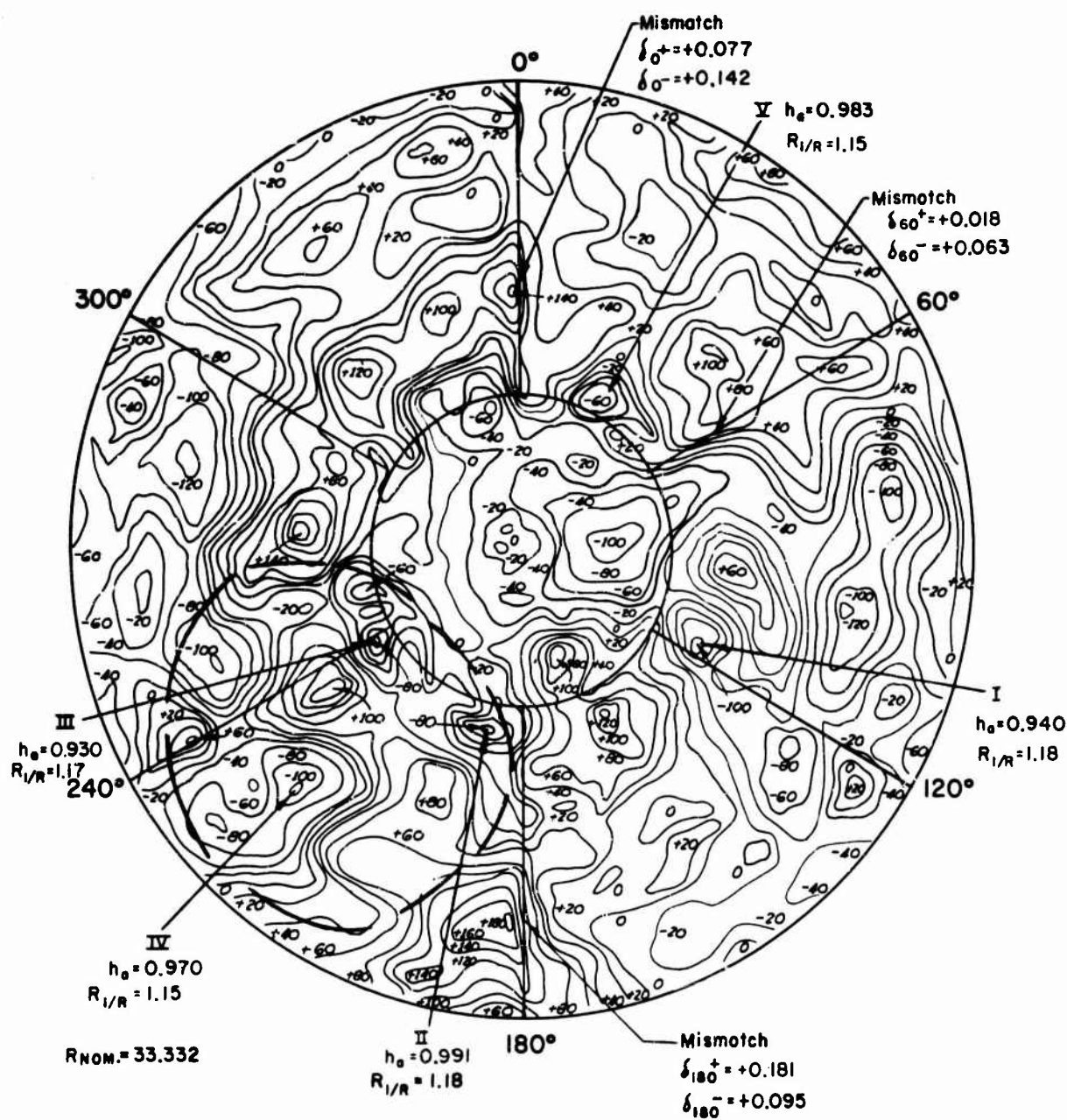


Figure 4g - Model 78

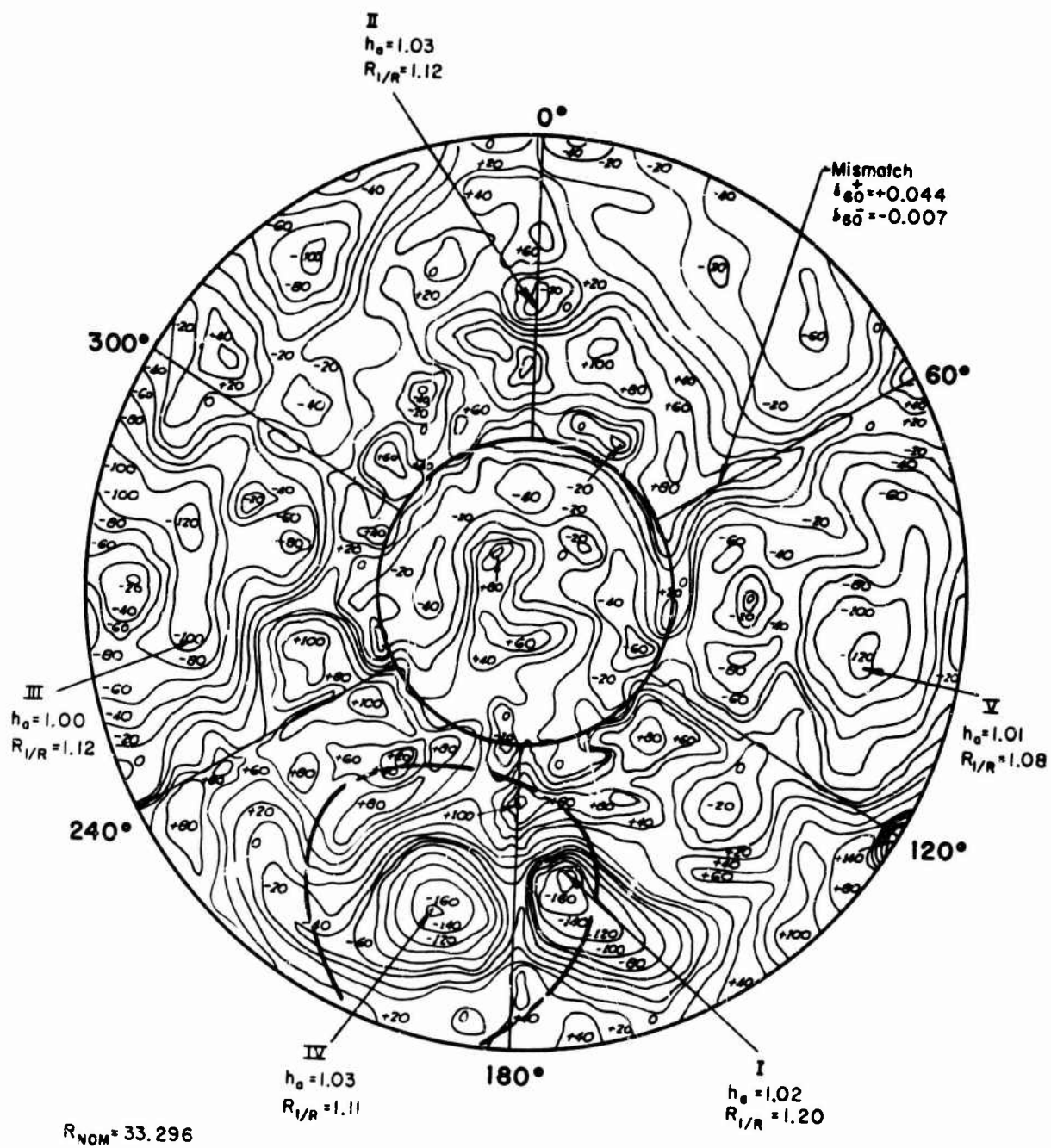


Figure 4h - Model 82

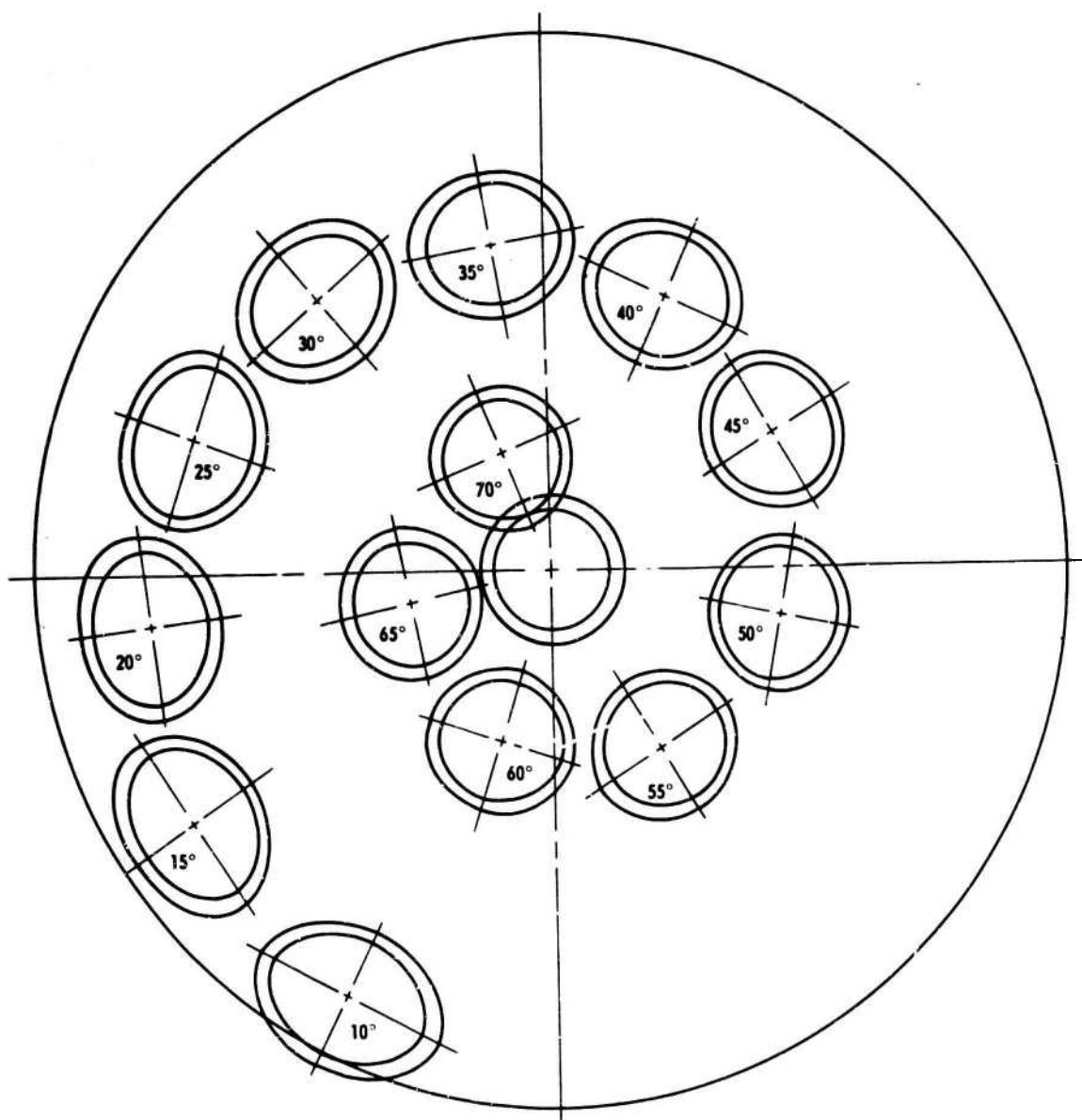


Figure 5 - Arc Length Scales

The surface enclosed by the solid circle shown represents a hemisphere unfolded into a flat surface whose radial scale remains constant.

Mismatch in terms of the deviations from sphericity are also given in Figure 4. It should be noted that in these plots no attempt was made to correct the midsurface shell contours for variations in shell thickness. In addition to the sphericity and mismatch readings, approximately 125 thickness measurements were taken on each model (see Table 2). These measurements indicated that during the pressing operation, the segments tended to thin out at the center and thicken at the edges. Moreover, grinding the welds also caused thickness variations at the edges of the segments. Thus, part of the variations in shell contours is attributable to thickness variations rather than to out-of-roundness of the shell.

The thickness measurements and contour maps were utilized to examine each model for critical local geometry. Each flat spot area was defined by its local thickness  $h_a$  and ratio of local to nominal radius  $R_l/R$ . A detailed description of the procedure is available in References 6 and 7 and is omitted here. Thickness variations were considered in utilizing the contour maps for out-of-roundness analysis. Although thickness variation influenced the overall shell contours, its effect over a critical arc length could be neglected in most cases.

#### TEST PROCEDURE

Each model was instrumented with approximately 70 foil-resistance strain gages. Areas for gaging were selected on the basis of flat spot calculations, mismatch data, and thickness readings. In some cases, gages were also placed near the juncture of sphere and cylinder. Strain-gage locations are presented in Figure 6.

The models were statically tested in oil in the 6-ft testing tank at the Model Basin. The test setup is presented in Figure 7. Generally, each test consisted of three pressure runs--the first and second to approximately 70 and 90 percent, respectively, of the collapse pressure and the third to collapse. Pressure was applied in increments, and each increment of pressure was held approximately 5 min. The final increment prior to collapse was less than 2 percent of the collapse pressure.

(Text continued on page 27.)

TABLE 2

## Measured Wall Thickness of the Models

		Meridional Orientation in Degrees						Circumferential Orientation in Degrees					
		0°	15	30	45	60°	90	0°	15	30	45	60°	90
Circumferential Orientation in Degrees	0°	0.800	0.800	0.818	0.815	0.797	0.783	0°	0.800	0.790	0.830	0.835	0.825
	15	0.797	0.797	0.800				15	0.818	0.820	0.820		
	30	0.818	0.805	0.795	0.790	0.805		30	0.830	0.817	0.790	0.800	0.805
	45	0.804	0.807	0.812				45	0.800	0.820	0.815		
	60°	0.784	0.808	0.794	0.812	0.803		60°	0.810	0.820	0.834	0.830	0.818
	75	0.778	0.810	0.765	0.818	0.790		75	0.817	0.808	0.804	0.818	0.788
	90	0.819	0.813	0.807	0.792	0.818		90	0.843	0.810	0.813	0.808	0.820
	105	0.807	0.815	0.817				105	0.805	0.815	0.815		
	120°	0.786	0.817	0.820	0.817	0.817		120°	0.805	0.815	0.825	0.818	0.805
	135	0.823	0.820	0.803	0.780	0.788		135	0.785	0.815	0.823	0.790	0.805
	150	0.820	0.809	0.800	0.796	0.811		150	0.834	0.823	0.820	0.814	0.820
Meridional Orientation in Degrees	165	0.800	0.800	0.811	0.803			165	0.805	0.817	0.815		
	180°	0.810	0.808	0.800	0.810	0.788		180°	0.834	0.834	0.830	0.834	0.800
	195	0.817	0.818	0.802	0.787	0.795		195	0.803	0.830	0.842	0.828	0.805
	210	0.825	0.812	0.797	0.785	0.803		210	0.837	0.818	0.804	0.818	0.795
	225	0.805	0.805	0.805				225	0.820	0.815	0.815		
	240°	0.790	0.800	0.822	0.807	0.795		240°	0.823	0.818	0.823	0.825	0.815
	255	0.813	0.824	0.810	0.829	0.810		255	0.820	0.820	0.820	0.823	0.810
	270	0.832	0.809	0.803	0.803	0.798		270	0.824	0.810	0.805	0.810	0.815
	285	0.822	0.810	0.503	0.807			285	0.820	0.809	0.810	0.810	
	300°	0.822	0.817	0.814	0.809	0.792		300°	0.820	0.800	0.822	0.825	0.792
	315	0.798	0.810	0.794	0.783	0.777		315	0.777	0.793	0.815	0.807	0.790
	330	0.825	0.808	0.803	0.787	0.815		330	0.827	0.815	0.810	0.807	0.805
	345	0.818	0.818	0.814				345	0.805	0.805	0.807	0.805	
	360°	0.800	0.785	0.825	0.820	0.795		360°	0.822	0.817	0.830	0.797	0.790
		h <sub>avg.</sub> = 0.806    h <sub>min.</sub> = 0.765    h <sub>max.</sub> = 0.832						h <sub>avg.</sub> = 0.814    h <sub>min.</sub> = 0.777    h <sub>max.</sub> = 0.843					
		Model 75						Model 79					

TABLE 2 - (Continued)

Circumferential Orientation in Degrees										Meridional Orientation in Degrees										Circumferential Orientation in Degrees										Meridional Orientation in Degrees									
0°	15	30	45	60°	60°	75	90	0°	15	30	45	60°	60°	75	90	0°	15	30	45	60°	60°	75	90	0°	15	30	45	60°	60°	75	90								
0°	0.802	0.795	0.807	0.820	0.785	0.810	0.797	0.765								0°	0.783	0.795	0.770	0.765	0.805	0.743	0.797	0.750	15	0.785	0.795	0.793											
15	0.800	0.810	0.810													30	0.820	0.800	0.782	0.787	0.773	0.800	0.793	30	0.820	0.800	0.782	0.787	0.773	0.800	0.793								
30	0.817	0.800	0.792	0.787	0.767	0.802	0.800									45	0.800	0.790	0.798					45	0.800	0.790	0.798												
45	0.795	0.803	0.795													60°	0.765	0.785	0.765	0.822	0.745	0.775	0.793	60°	0.765	0.785	0.765	0.822	0.745	0.775	0.793								
60°	0.790	0.790	0.807	0.796	0.777	0.798	0.800									60°	0.805	0.803	0.790	0.803	0.830			60°	0.805	0.803	0.790	0.803	0.830										
60°	0.803	0.805	0.822	0.800	0.795											75	0.800	0.800	0.800	0.783				75	0.800	0.800	0.800	0.783											
75	0.805	0.805	0.805	0.797												90	0.823	0.795	0.783	0.787	0.715	0.778	0.793	90	0.795	0.783	0.787	0.715	0.778	0.793									
90	0.820	0.798	0.787	0.792	0.750	0.805	0.800									105	0.800	0.800	0.800	0.796				105	0.800	0.800	0.800	0.796											
105	0.805	0.815	0.806													120°	0.773	0.845	0.800	0.787	0.755	0.775	0.797	120°	0.773	0.845	0.800	0.787	0.755	0.775	0.797								
120°	0.803	0.817	0.802	0.793		0.802	0.795									120°	0.783	0.855	0.810	0.773	0.850			120°	0.783	0.855	0.810	0.773	0.850										
120°	0.798	0.820	0.804	0.788												135	0.800	0.790	0.795					135	0.800	0.790	0.795												
135	0.804	0.797	0.793													150	0.825	0.790	0.787	0.787	0.740	0.787	0.793	150	0.825	0.790	0.787	0.787	0.740	0.787	0.793								
150	0.827	0.794	0.782	0.784	0.773	0.800	0.796									165	0.805	0.805	0.805					165	0.805	0.805	0.805												
165	0.795	0.797	0.795													180°	0.765	0.755	0.785	0.795	0.835	0.770	0.797	180°	0.765	0.755	0.785	0.795	0.835	0.770	0.797								
180°	0.797	0.797	0.803	0.803	0.774	0.807	0.800									180°	0.793	0.795	0.815	0.810	0.702			180°	0.793	0.795	0.815	0.810	0.702										
180°	0.810	0.802	0.804	0.802	0.778											195	0.792	0.800	0.800					195	0.792	0.800	0.800												
195	0.797	0.790	0.789													210	0.816	0.795	0.792	0.790	0.763	0.778	0.793	210	0.816	0.795	0.792	0.790	0.763	0.778	0.793								
210	0.820	0.802	0.787	0.778	0.790	0.803	0.797									225	0.797	0.797	0.797					225	0.797	0.797	0.797												
225	0.810	0.803	0.797													240°	0.777	0.765	0.787	0.787	0.780	0.777	0.795	240°	0.777	0.765	0.787	0.787	0.780	0.777	0.795								
240°	0.790	0.803	0.812	0.800	0.760	0.807	0.797									240°	0.750	0.785	0.787	0.790	0.850			240°	0.750	0.785	0.787	0.790	0.850										
240°	0.802	0.797	0.812	0.804	0.795											255	0.805	0.802	0.800					255	0.805	0.802	0.800												
255	0.787	0.792	0.794													270	0.827	0.790	0.787	0.785	0.820	0.777	0.792	270	0.827	0.790	0.787	0.785	0.820	0.777	0.792								
270	0.810	0.796	0.783	0.793	0.797	0.813	0.798									285	0.805	0.805	0.790	0.793				285	0.805	0.805	0.790	0.793											
285	0.796	0.795	0.795													300°	0.790	0.795	0.770	0.780	0.770	0.772	0.792	300°	0.790	0.795	0.770	0.780	0.770	0.772	0.792								
300°	0.797	0.807	0.814	0.812	0.803	0.813	0.805									300°	0.785	0.787	0.780	0.790	0.775			300°	0.785	0.787	0.780	0.790	0.775										
300°	0.797	0.793	0.808	0.805	0.773											315	0.793	0.790	0.790	0.800				315	0.793	0.790	0.790	0.800											
315	0.785	0.793	0.815													330	0.828	0.792	0.768	0.780	0.743	0.775	0.792	330	0.828	0.792	0.768	0.780	0.743	0.775	0.792								
330	0.807	0.790	0.780	0.787	0.792											345	0.803	0.800	0.800	0.793				345	0.803	0.800	0.800	0.793											
345	0.792	0.793	0.800													360°	0.845	0.775	0.728	0.720	0.750			360°	0.845	0.775	0.728	0.720	0.750										
360°	0.796	0.790	0.807	0.807	0.775											h <sub>avg.</sub> = 0.789    h <sub>min.</sub> = 0.702    h <sub>max.</sub> = 0.855																							

Model 76

Model 80



TABLE 2 - (Continued)

Meridional Orientation in Degrees										Circumferential Orientation in Degrees									
0°	15	30	45	60°	75	90	0°	15	30	45	60°	75	90						
0°	1.000	1.025	1.000	1.020	0.977	0.990	0°	1.015	1.020	1.035	1.040	1.030	0.985						
15	1.003	1.002	1.004				15	1.015	1.015	1.000	1.015								
30	1.050	1.010	1.000	0.985	0.992		30	1.050	1.020	1.000	1.000	1.015	1.005						
45	1.017	1.012	1.008				45	1.020	1.020	1.023	1.125								
60°	1.004	1.005	0.970	0.963	1.030		60°	1.025	1.005	1.035	1.025	1.025	1.001						
60°	1.000	1.005	1.009	1.020	1.005		60°	1.020	1.015	1.030	1.030	1.020							
75	1.010	1.012	1.022				75	1.020	1.020	1.000	1.025								
90	1.025	1.010	1.010	1.012	1.025		90	1.055	1.010	1.000	1.010	0.995	1.000						
105	1.010	1.010	1.010	1.015			105	1.115	1.115	1.110	1.030								
120°	0.980	0.958	0.995	0.997	0.993		120°	0.980	1.025	1.055	1.045	0.995	1.000						
120°	1.030	1.018	1.018	1.015	0.990		120°	1.035	1.035	1.045	1.045	1.000							
135	1.015	1.015	1.015	1.012			135	1.025	1.025	1.015	1.025								
150	1.055	1.020	1.008	0.995	0.985		150	1.055	1.025	1.015	0.995	1.010	1.010						
165	1.015	1.015	1.015	1.015			165	1.015	1.015	1.020	1.025								
180°	0.980	1.000	1.015	1.020	0.975		180°	1.015	1.055	1.025	1.055	1.025	1.015						
180°	1.013	1.005	1.015	1.018	0.993		180°	1.015	1.025	1.040	1.040	0.995							
195	1.005	0.998	1.003				195	1.020	1.020	1.010	1.020								
210	1.025	1.012	0.990	0.988	0.983		210	1.050	1.015	1.010	1.010	1.020	1.015						
225	1.018	1.005	1.008				225	1.020	1.020	1.000	1.015								
240°	0.993	1.010	1.010	0.970	0.970		240°	1.035	1.030	1.010	1.030	1.015	1.015						
240°	1.020	1.008	1.018	1.015	0.975		240°	1.015	1.030	1.030	1.020	1.015							
255	1.010	1.007	1.005				255	1.025	1.025	1.010	1.020								
270	1.035	1.015	1.000	0.983	1.000		270	1.050	1.010	0.990	1.005	1.010	1.010						
285	1.008	1.012	1.014				285	1.020	1.020	1.015	1.025								
300°	1.010	1.010	1.015	1.005	0.990		300°	1.035	1.035	1.055	1.030	1.000	1.015						
300°	1.015	1.028	1.040	1.035	0.998		300°	1.025	1.030	1.040	1.040	0.985							
315	1.012	1.005	1.010				315	1.015	1.015	1.010	1.025								
330	1.012	1.003	0.997	1.000	1.022		330	1.050	1.015	1.015	1.020	1.015	1.010						
345	1.005	1.008	1.010				345	1.020	1.020	1.015	1.020								
360°	0.993	1.008	0.993	1.009	0.987		360°	0.985	1.000	1.030	1.045	1.015							
$h_{avg.} = 1.006$						$h_{min.} = 0.970$	$h_{avg.} = 1.022$						$h_{min.} = 0.980$	$h_{max.} = 1.055$					

Model 77

Model 81



TABLE 2 - (Continued)

Meridional Orientation in Degrees										Meridional Orientation in Degrees									
0°	15	30	45	60°	60°	60°	75	90	0°	15	30	45	60°	60°	60°	75	90		
0°	0.985	1.010	1.000	1.000	0.975	0.975	0.975	0.982	0°	0.990	1.005	1.035	1.030	1.025	0.988	1.010	0.998		
15	1.018	1.015	1.020						15	1.020	1.012	1.005							
30	1.040	1.015	1.000	1.020	0.900	1.000	1.000		30	1.045	1.020	1.005	0.995		1.008	1.005			
45	1.010	1.010	1.020	1.015					45	1.020	1.005	1.010							
60°	1.010	1.015	0.990	1.010	0.980	1.005	1.020		60°	0.995	1.012	1.018	1.035	0.985	1.015	0.990			
60°	0.895	1.015	0.985	1.010	0.900				60°	1.010	1.025	0.985	1.040	0.990					
75	1.015	1.005	1.015						75	1.015	1.015	1.030							
90	1.030	1.005	0.988	1.000	0.993	1.030	1.010		90	1.020	1.010	1.015	0.998	1.005	1.010	1.020			
105	1.013	1.000	1.010						105	1.005	1.005	1.010	1.022						
120°	0.995	1.010	0.970	0.980	0.910	0.950	1.000		120°	1.010	1.015	1.035	1.020	0.980	0.950	1.000			
120°	0.890	1.000	0.975	0.860	0.950				120°	1.025	1.005	1.055	1.055	1.030					
135	0.892	1.010	1.013						135	1.020	1.020	1.020							
150	1.040	1.010	0.975	0.990	0.968	0.958	1.012		150	1.040	1.020	1.000	0.990	1.030	1.020	1.015			
165	1.020	1.010	1.003						165	1.035	1.020	1.030							
180°	0.990	0.995	0.990	0.971	0.978	0.980	1.000		180°	1.020	1.030	1.035	1.038	0.990	1.010	1.015			
180°	1.000	0.965	0.970	0.970	0.985				180°	1.020	0.955	0.945	1.025	1.035					
195	1.020	1.013	1.018						195	1.030	1.020	1.025							
210	0.940	1.005	0.990	0.970	0.980	1.008	1.010		210	1.040	1.010	1.000	0.995	1.015	1.030	1.018			
225	1.015	1.010	1.015						225	1.020	1.000	1.000							
240°	1.005	1.015	0.990	0.970	0.985	0.968	1.015		240°	0.985	1.000	1.030	1.030	0.980	1.005	1.010			
240°	0.990	0.990	0.975	0.950	0.920				240°	0.955	1.000	1.010	1.030	0.990					
255	1.015	1.015	1.015						255	1.005	1.005	1.005							
270	0.945	1.005	0.997	0.998	0.985	1.005	1.015		270	1.020	1.000	0.990	1.000	1.008	1.005	1.008			
285	1.005	1.010	1.010						285	1.008	1.000	1.025							
300°	1.000	0.960	1.015	0.990	0.960	1.005	1.010		300°	0.980	1.020	1.025	1.040	1.000	0.970	1.008			
300°	0.970	0.970	1.010	0.988	0.970				300°	1.030	1.028	1.045	1.040	0.990					
315	1.020	1.018	1.025						315	1.025	1.010	1.022							
330	1.040	1.020	1.008	1.000	0.975	0.995	1.003		330	1.038	1.015	1.000	1.005	1.010	0.970	1.010			
345	1.005	1.015	1.010						345	1.010	1.025	1.020							
360°	1.000	1.010	1.018	0.985	0.875				360°	1.030	0.995	1.020	1.025	0.968					
h <sub>avg.</sub> = 0.992    h <sub>min.</sub> = 0.860    h <sub>max.</sub> = 1.040									h <sub>avg.</sub> = 1.012    h <sub>min.</sub> = 0.945    h <sub>max.</sub> = 1.045										
Model 78									Model 82										

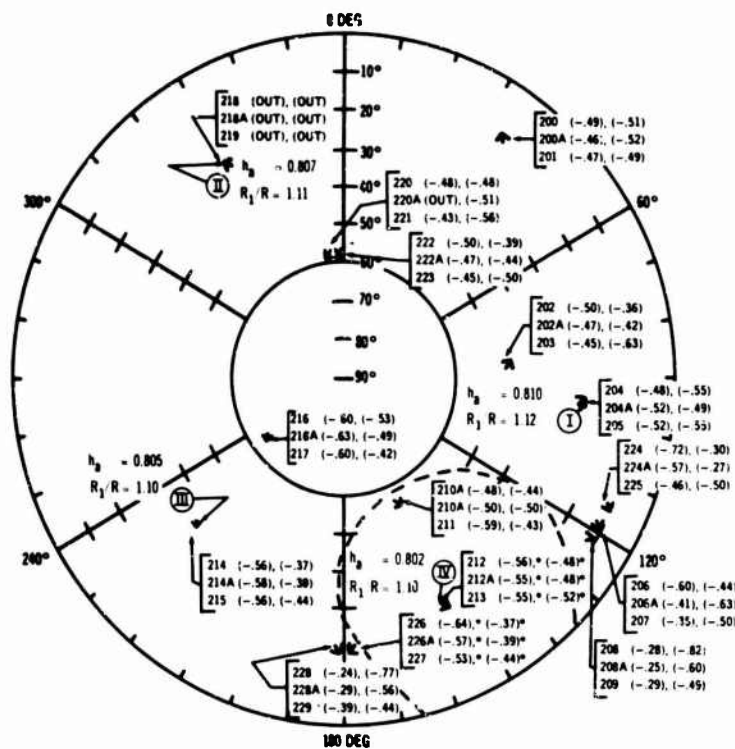


Figure 6a - Model 75

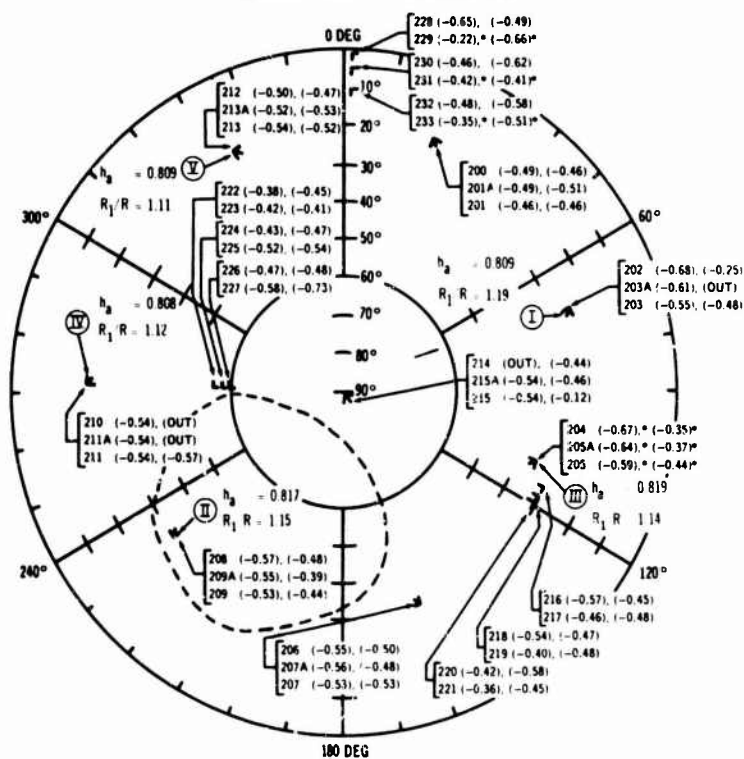


Figure 6b - Model 79

Figure 6 - Strain-Gage Locations and Strain Sensitivities

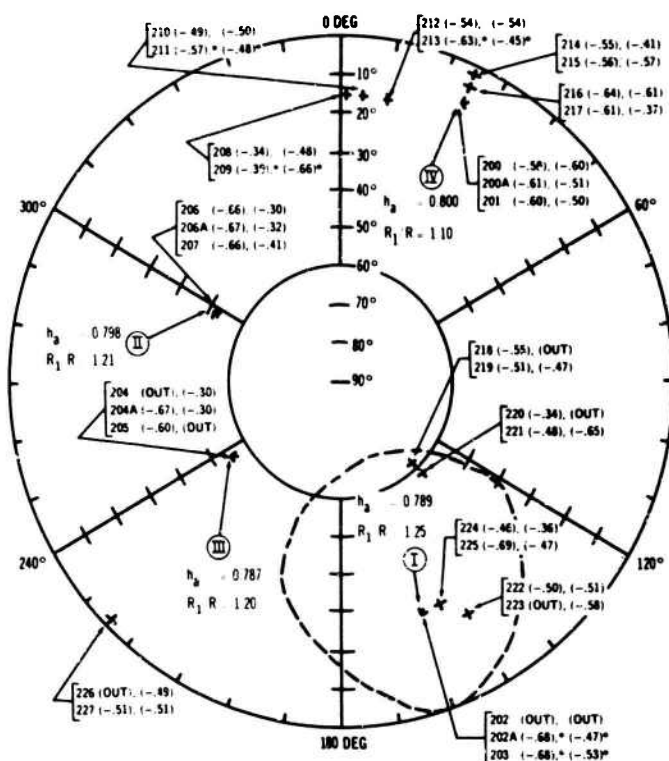


Figure 6c - Model 76

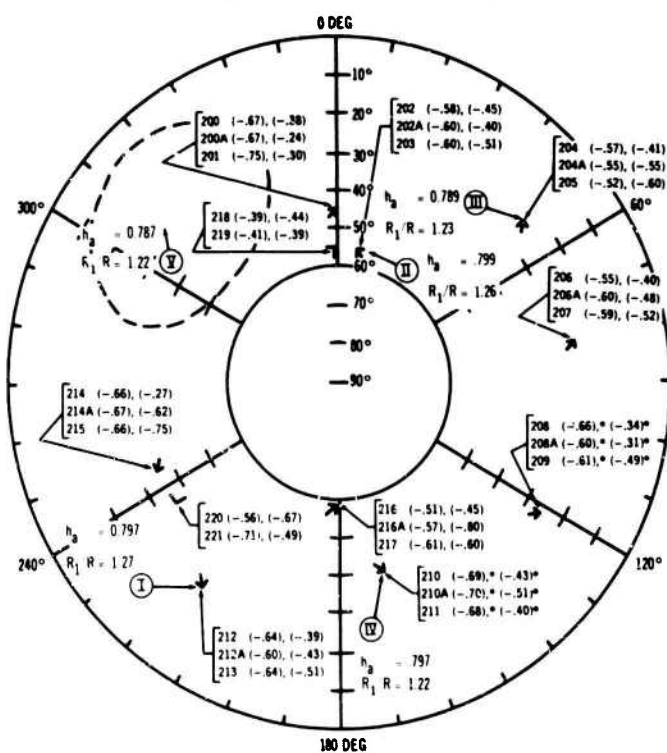


Figure 6d - Model 80

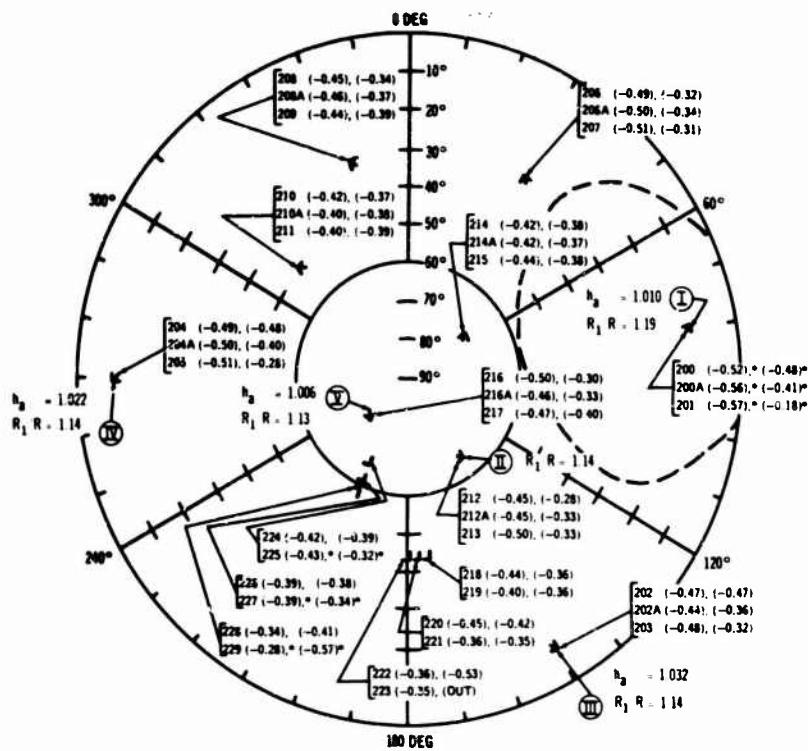


Figure 6e - Model 77

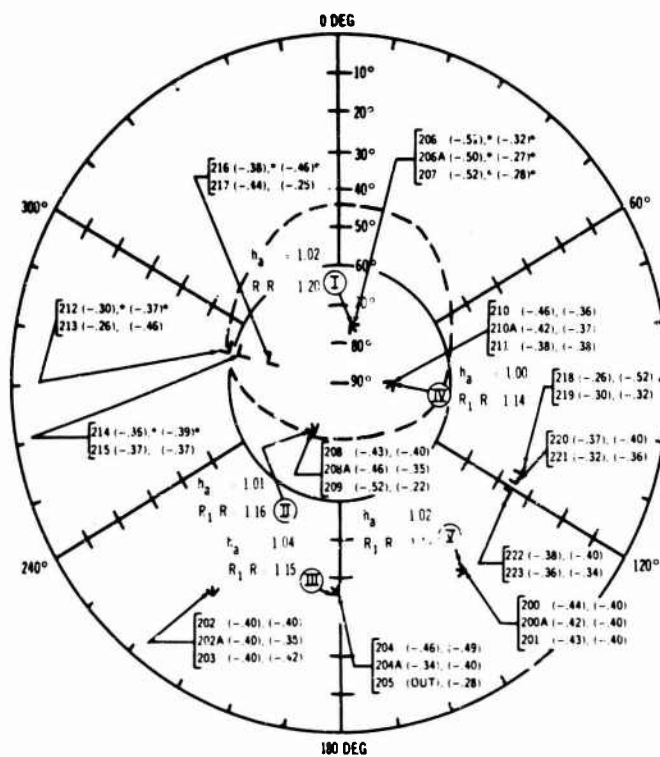


Figure 6f - Model 81

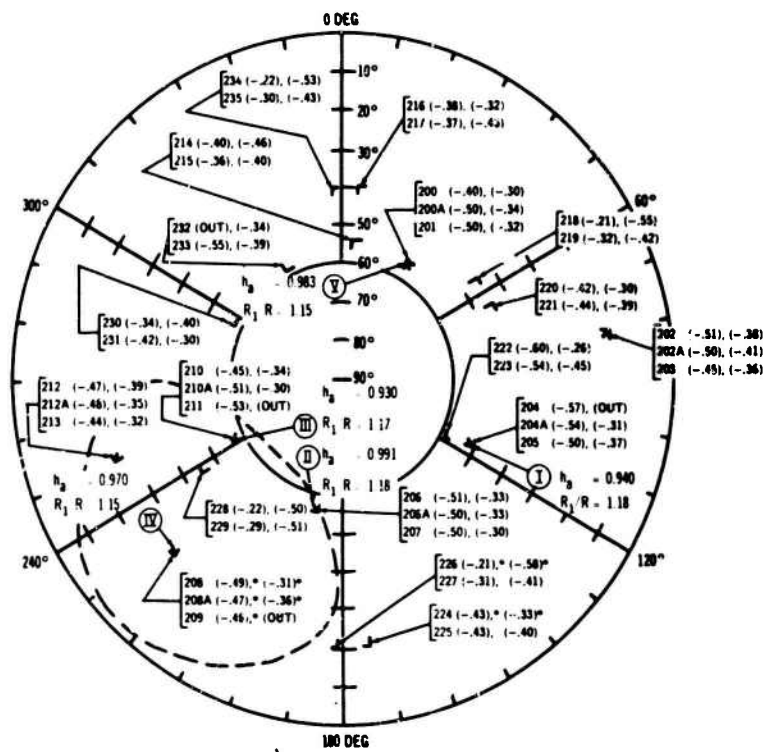


Figure 6g - Model 78

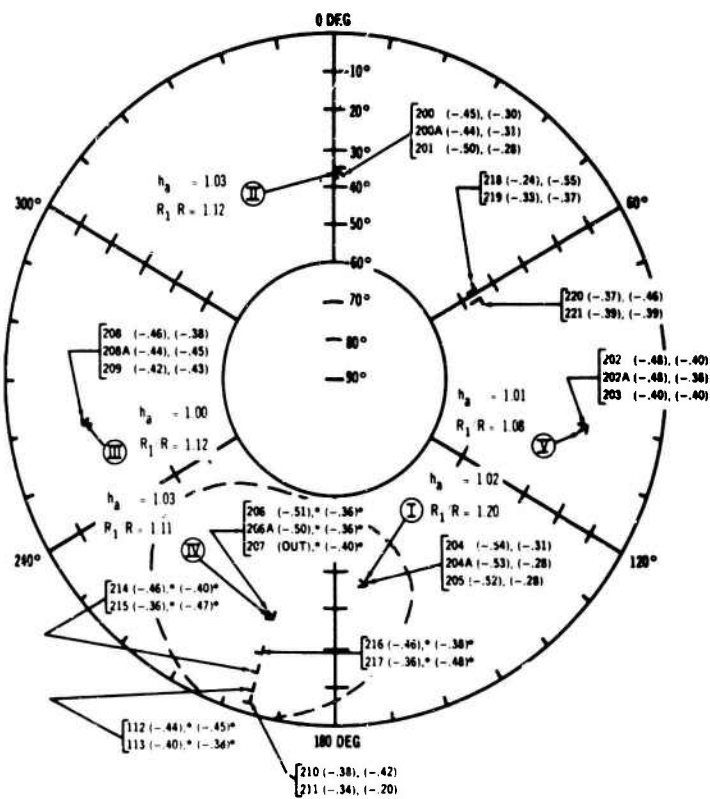


Figure 6h - Model 82

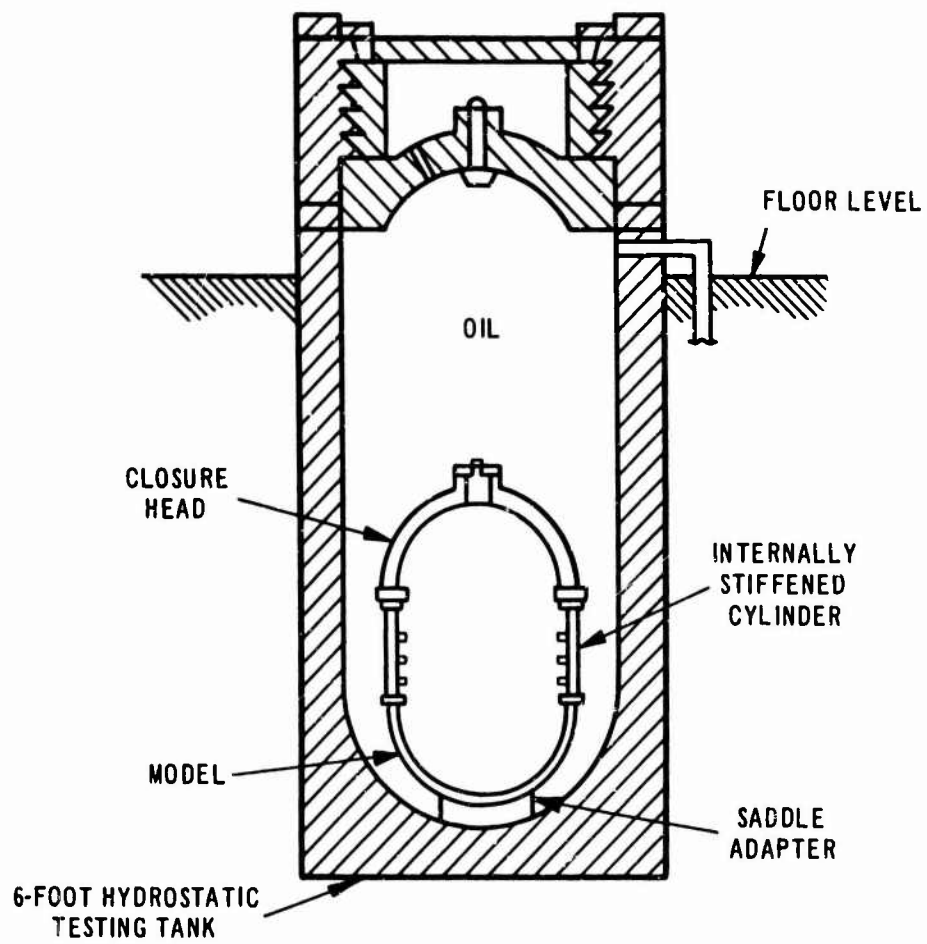


Figure 7 - Test Setup

## RESULTS AND DISCUSSION

Experimental collapse pressures for each model are shown in Table 3. Strain sensitivities are shown in Figure 6, and typical pressure-strain plots are given in Figure 8. Figure 9 shows the models after collapse.

Nondimensional plots of experimental results for the eight models are presented in Figure 10; the abscissa is the ratio of elastic buckling pressure  $P_3'$  to the yield pressure  $P_y'$ , and the ordinate is the ratio of the experimental collapse pressure  $P_c$  to  $P_y'$ . It should be noted that local geometry in the area of failure was used to calculate  $P_3'$  and  $P_y'$ , which are defined by the expressions

$$P_3' = 0.84E \left( \frac{h_a}{R_{10}} \right)^2 \quad \text{for } \nu = 0.3 \quad [1]$$

$$P_y' = \frac{2 \sigma_y h_a R_{1m}}{(R_{10})^2} \quad [2]$$

where  $h_a$  is the average thickness at the flat spot,  
 $R_{10}$  is the local outside radius,  
 $R_{1m}$  is the local midsurface radius,  
 $E$  is Young's modulus, and  
 $\sigma_y$  is the yield strength.

Results of Reference 6 have been included for comparison. It can be observed that the present results are in excellent agreement with previous trends for both as-fabricated and stress-relieved models. The difference between the yield line and the lower bound for the stress-relieved models is attributed to the effect of secondary moments. It appears that this effect becomes negligible as the shells attain margins of stability ( $P_3'/P_y'$ ) of three and greater. The difference between the lower bound trends for stress-relieved and as-fabricated models is attributed to the presence of residual stresses. As the shells become more stable, the effect of residual stresses on collapse strength decreases. It is significant to note the collapse pressures obtained in these eight tests could be predicted within 10 percent by utilizing the imperfection analysis and simply extrapolating test results of Reference 6.

(Text continued on page 34.)

Figure 8 - Typical Pressure-Strain Plots

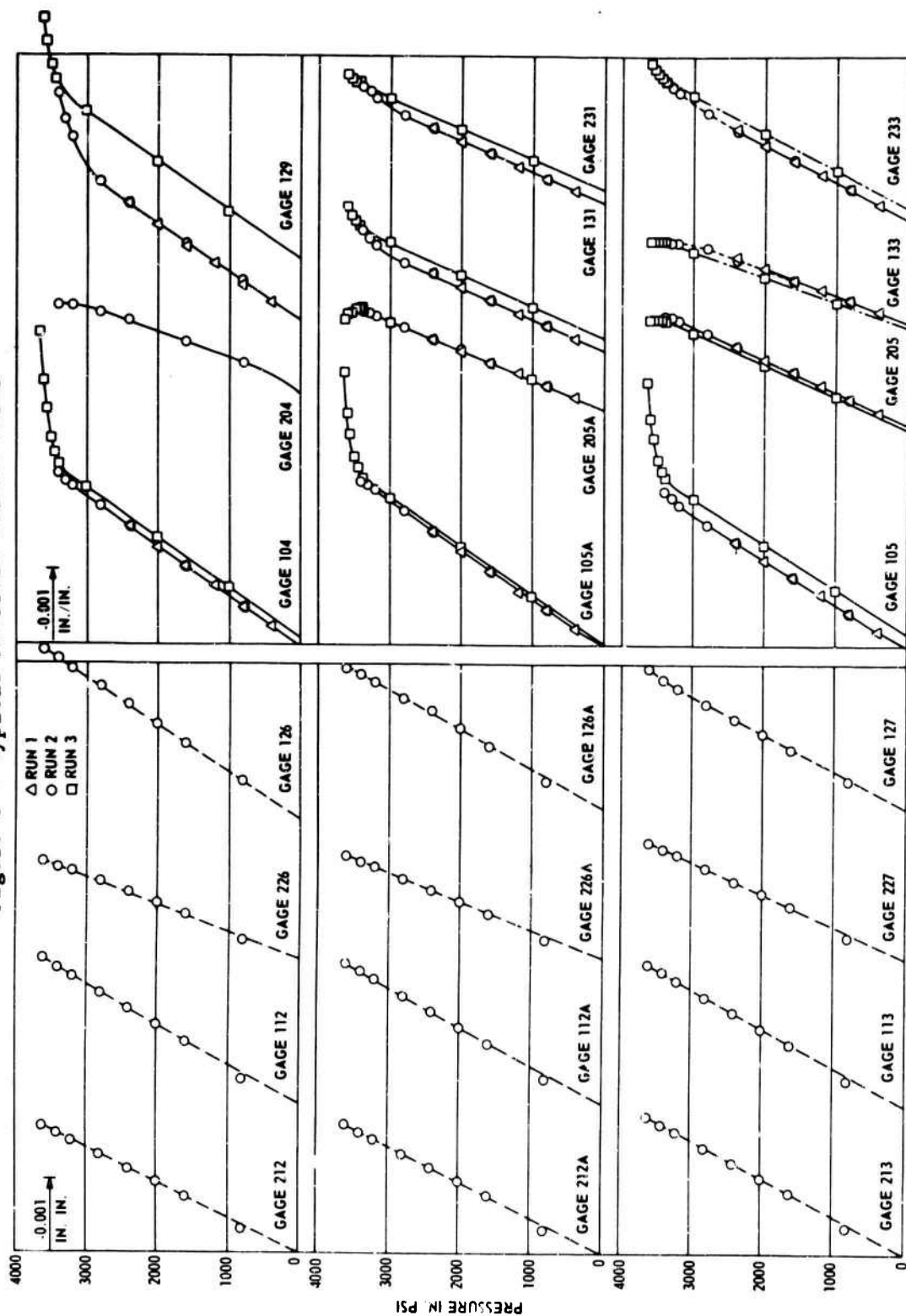


Figure 8a - Model 75

Figure 8b - Model 79



Figure 8 (Continued)

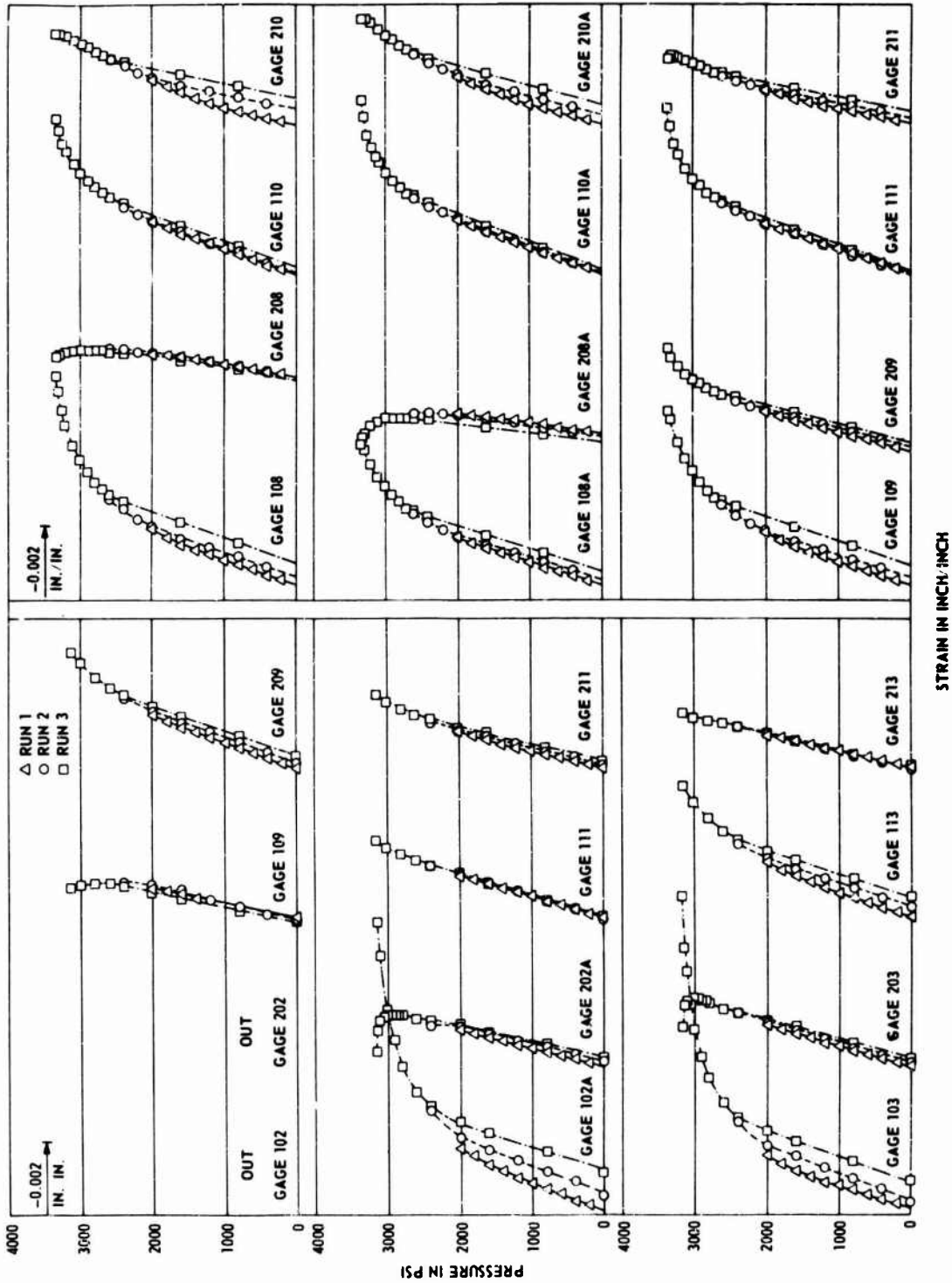


Figure 8d - Model 80

Figure 8c - Model 76

Figure 8 (Continued)

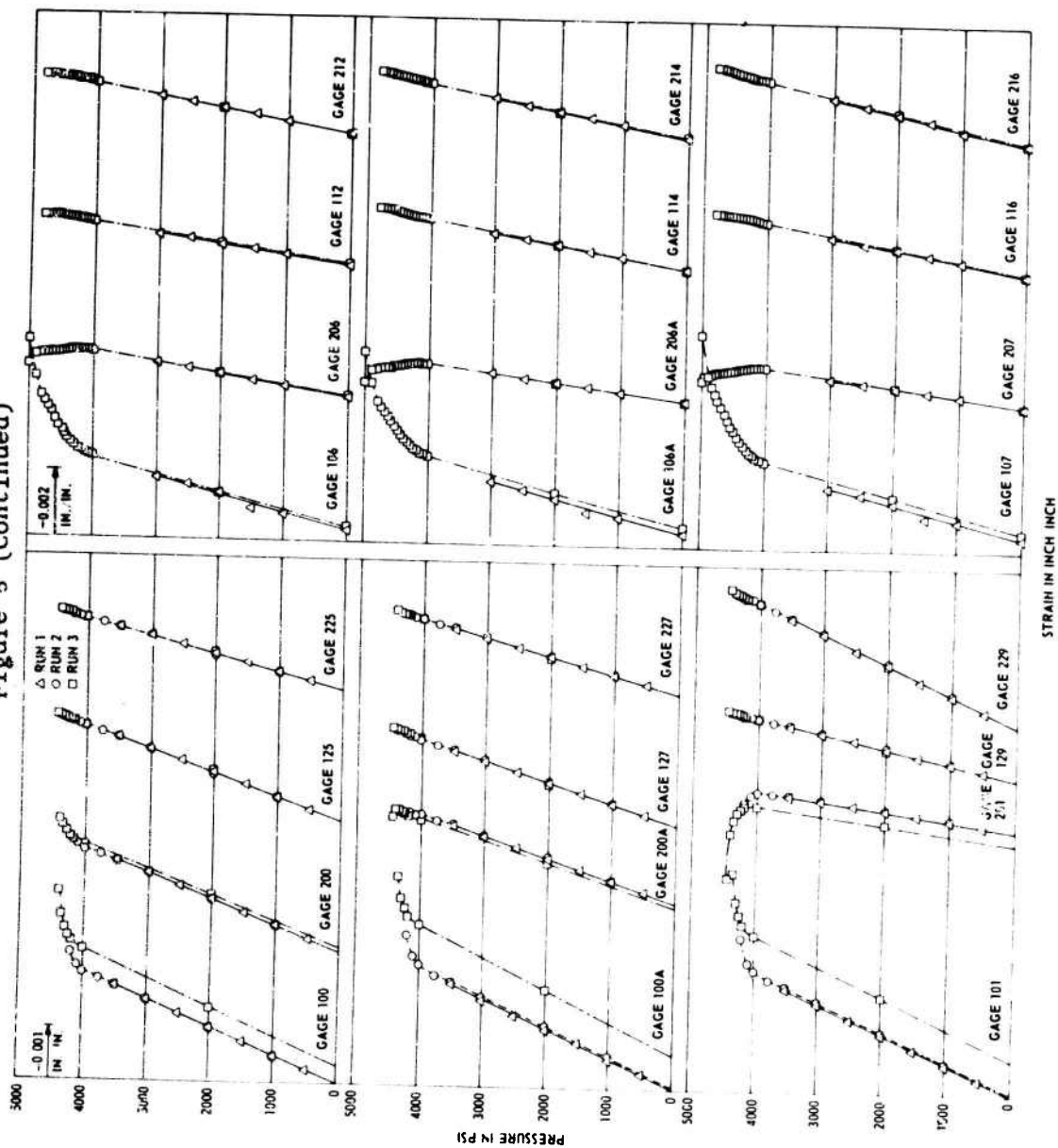


Figure 8e - Model 77

Figure 8f - Model 81

Figure 8 (Continued)

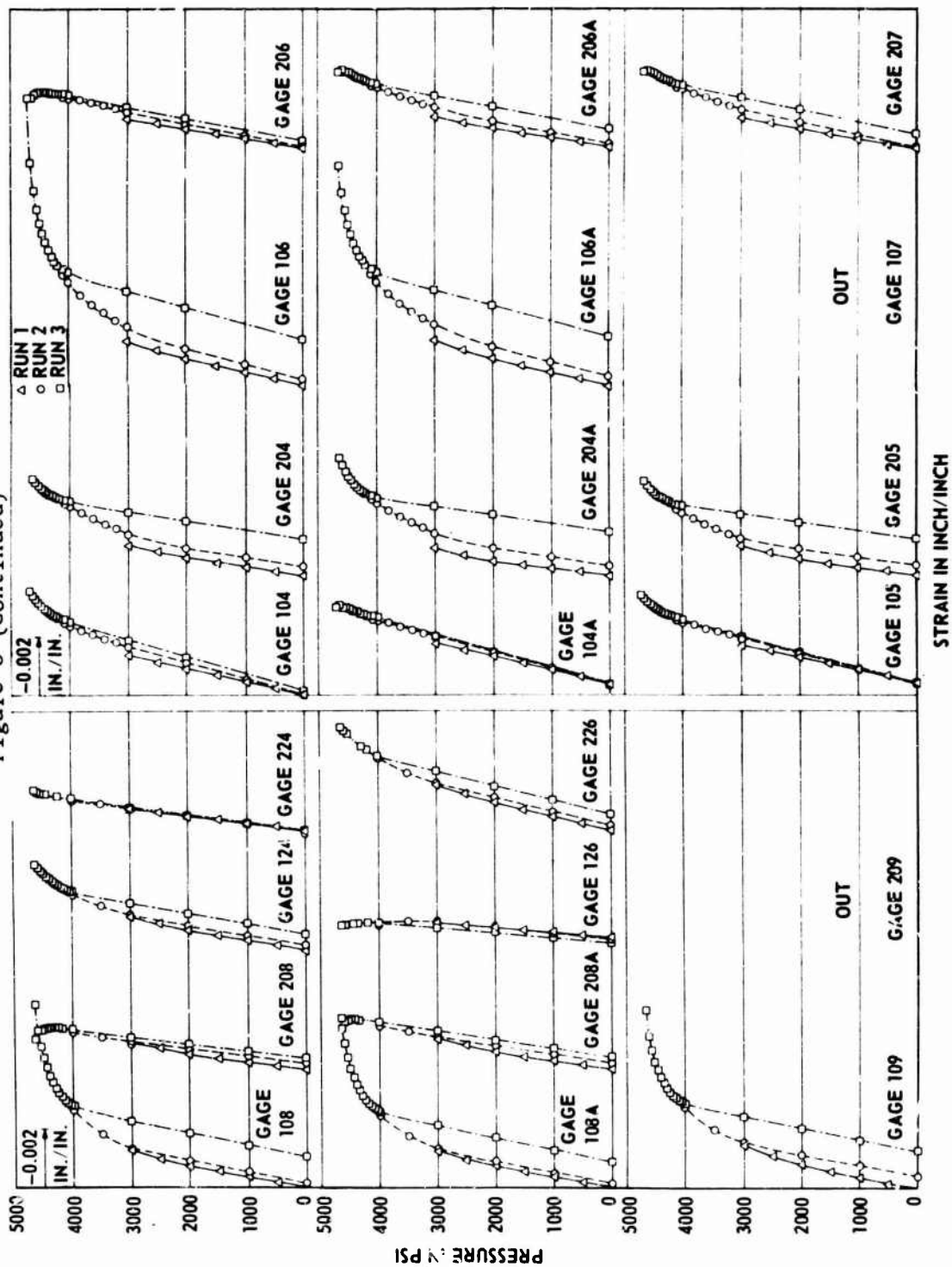


Figure 8g - Model 78

Figure 8h - Model 82

Figure 9 - Models after Collapse



Figure 9a - Model 75

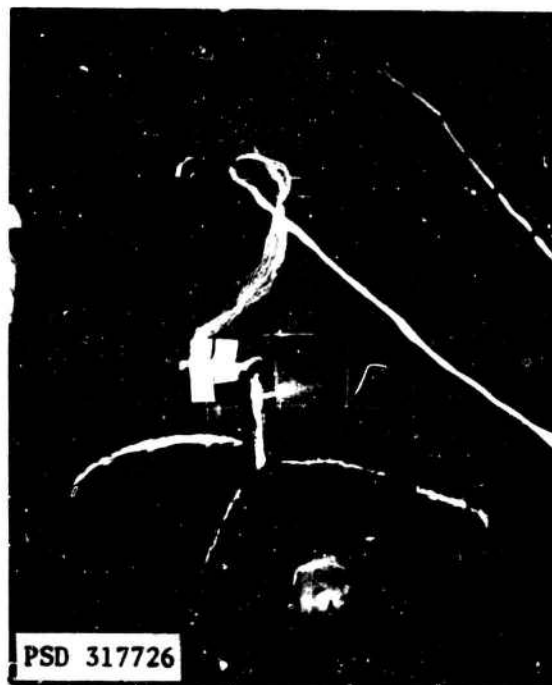


Figure 9b - Model 79

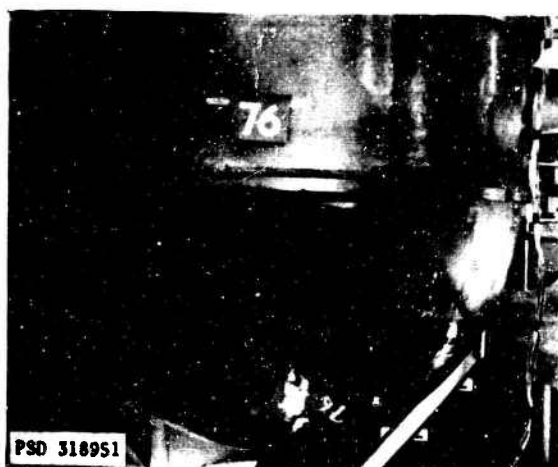


Figure 9c - Model 76



Figure 9d - Model 80



Figure 9e - Model 77

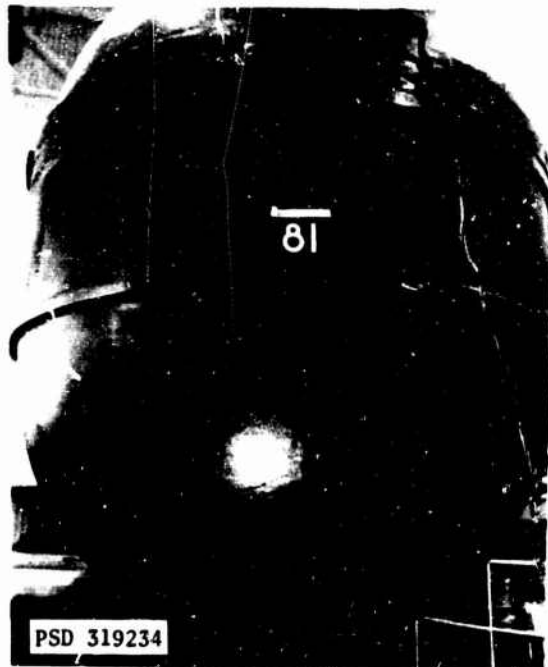


Figure 9f - Model 81

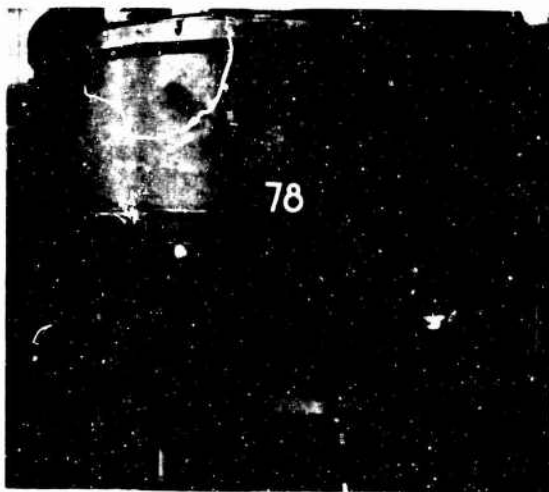


Figure 9g - Model 78



Figure 9h - Model 82

Mismatch on the models could be considered excessive from the viewpoint of possible submarine fabrication tolerances. In most cases, a maximum mismatch of approximately 0.1 in., or roughly 10 percent of the shell thickness, was observed. This caused bending stresses which ranged from 20 to 45 percent of the membrane stress. Unfortunately, the effect of mismatch on collapse strength is somewhat obscured by other variables, and to try to separate its effect is not practical at this time. It should be noted, however, that any effect of mismatch on the strength of the models is reflected in the curves of Figure 10.

On Model 82 (not stress relieved), the question may be raised as to why the result was plotted using the local geometry at IV rather than I (minimum  $h_a/R_{10}$ ), since both are included in the failure envelope (see Figure 6). Strain measurements taken in these two areas suggest that failure was caused by the flat spot at IV. The higher elastic membrane strains were recorded at IV, and the inelastic strains in this area started to "run" just prior to collapse. Thus, the result for Model 82 was plotted utilizing the local geometry at IV.

The imperfection analysis utilized in evaluating these models admittedly has limitations. For example, failure of some of these models did not occur in the geometrically critical area (minimum  $h_a/R_{10}$ ). This may be attributed to such factors as varying residual stresses, yield strength, shape of the stress-strain curve, shape of the imperfections, mismatch, and boundary conditions which, at present, are neglected in the analysis. However, the presentation of the data in the form of Figure 10, where each datum point is plotted utilizing the geometry in the area of failure, makes it possible to observe the combined effect of the variables.

In plotting the results of this series of tests for the as-fabricated models, the yield strengths used in conjunction with Equation [2] were determined from material of the original plate.\* Discussion in Reference 6 notes that the yield strengths of the original plate material

---

\* The data points in Figure 10, which represent the results of the 66-in. diameter models of Reference 6 are based on values of yield strength determined after test, since available yield strength data for the original plating is inadequate.

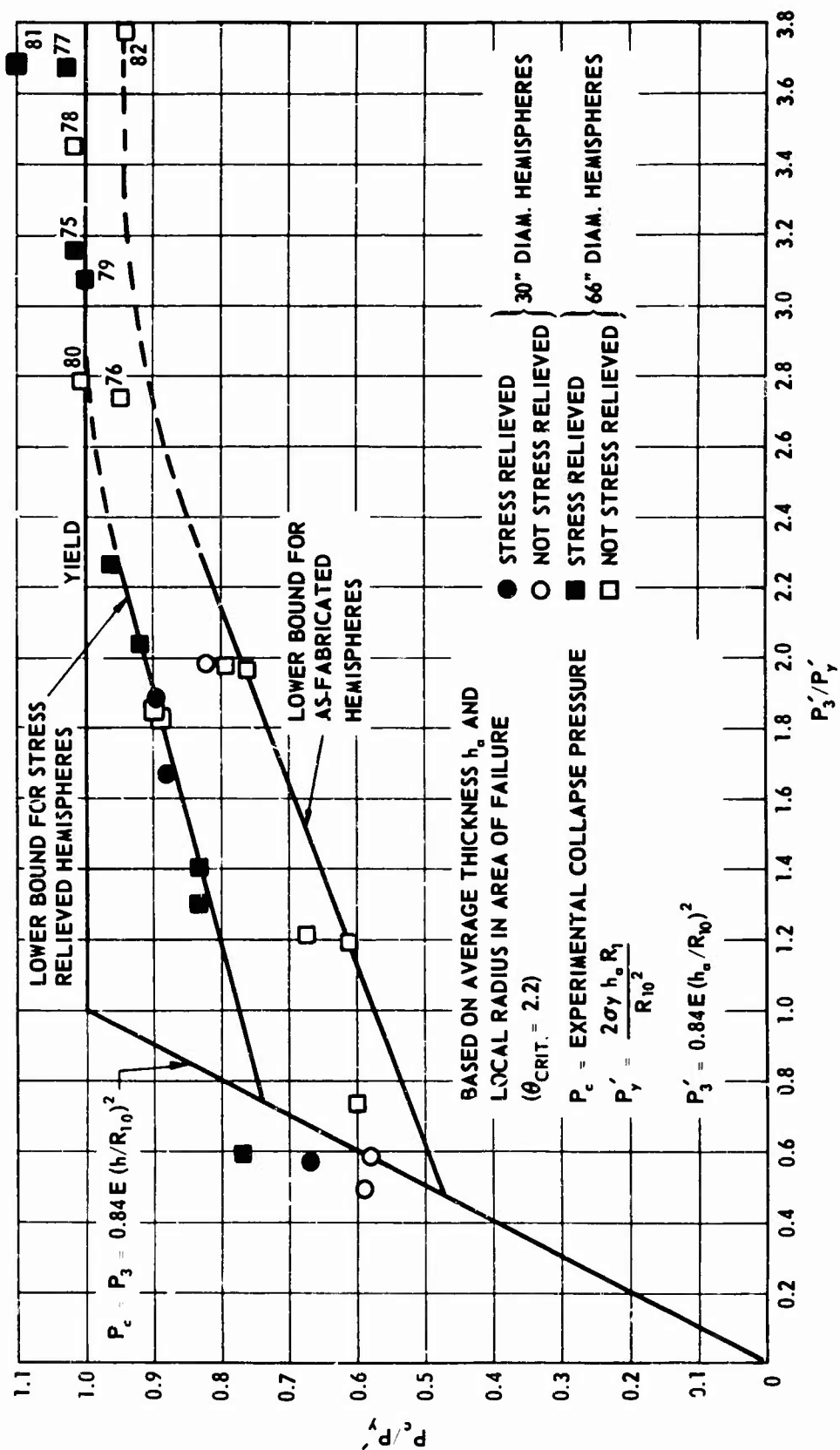


Figure 10 - Nondimensional Plot of Experimental Results for Fabricated HY-80 Steel Spherical Shells

may not be representative of the material in place. The yield strengths of the as-fabricated models were generally 10 percent higher than the stress-relieved models. Since this would affect the position of the data points in Figure 10, it was decided to make a limited investigation of forming on the strength of the material. Specimens were taken from a skirt segment of Model 82 (not stress relieved) between the 0- and 60-deg generators, which appeared to be an area of relatively low stress. The specimen location and test results are presented in Figure 3. Specimens from the model and the original plate were 1/2 in. in diameter by 2 in. in length. For each specimen location, except the center, the yield strength was increased in the direction parallel to the proximate edge and was decreased in the direction normal to it. No significant change in strength was observed at the center of the segment. These results appear to be in contrast with the observations made in Reference 6. Although a maximum increase in strength of 11 percent in the circumferential direction was observed, the strength of the segment in general was not increased by as much as 10 percent. As a matter of fact, if the strength in both directions is averaged for each location as was done in Reference 6, no significant change in strength would be obtained. A closer and more systematic investigation of the effect of forming on the strength of the material is currently in progress. Spherical skirt segments 66 in. in diameter and of varying thicknesses will be fabricated and tested. When these tests are completed, a much clearer understanding of the effect of forming will be obtained.

Typical stress-strain curves of the original plate and from the material in place for Model 82 are presented in Figure 2. Note that in each case cold working of the material altered the shape of the stress-strain curve from one that was essentially elastic and ideally plastic to a curvilinear type. It should be kept in mind that, in machining specimens from the model after testing, stresses are relieved at the free surfaces of the specimens thus making the resulting stress-strain curves only approximate representations of conditions within the model. The effect of residual stress on the elastic behavior of the shell can be observed in the pressure-strain plots presented in Figure 8. The strains



in the as-fabricated models become nonlinear at fairly low pressures, whereas the strains in the stress-relieved models remain linear at much higher pressures.

Table 3 compares experimental membrane stress sensitivities at flat spots with values calculated with local imperfection geometry. In most cases the agreement was within 10 percent, with the calculated stresses generally being higher than the measured values. The maximum difference obtained was 14 percent. Considering the relative severity of some of the assumptions made in the analysis (e.g., neglecting nonsymmetric imperfections), the agreement can be considered to be fairly good. At the present time, further study is being conducted on flat spots upon which refinements to the analysis can be based.

Up to the present time, designers of spherical shells have been seriously hampered by the lack of rational design guidance. The preliminary evaluation of the eight model tests, combined with the results of previous tests in the less stable regions, provides the designer with some of these critically needed tools. When the results are presented in the form of Figure 10, the combined effect of the variables--such as residual stress, mismatch, and boundary conditions--can be observed. The curves presented emphasize lower bound strength of test results and are applicable to the realistic design of fabricated spherical shells. At the present time, the effects of flat spots, residual stresses, and mismatch are being investigated both analytically and experimentally. On completion of these investigations, the results of the fabricated HY-80 spherical shells will be reevaluated, and the analysis will be refined. In addition to these studies, the behavior of spherical shells fabricated from materials with strain-hardening characteristics is being investigated.

#### CONCLUSIONS

1. It was possible to predict within 10 percent the collapse pressures of the eight models tested by utilizing imperfection analysis and extrapolating previous test results of less stable geometries.
2. The test results, when plotted in the form of Figure 10, provide the designer with a reasonable collapse equation for as-fabricated and

TABLE 3

## Local Geometry and Comparison of Calculated and Measured Membrane Stresses and Collapse Pressures

Model	Area	$h_a$ inch	$\frac{R_1}{R}$	Calculated Max. Membr. Stress Sens.* psi/psi	Measured Max. Membr. Stress Sens.** psi/psi	Ratio of Calc. to Meas. Stress	Experimental Collapse psi
75***	I	0.810	1.12	23.5	22.2	1.06	3800
	II	0.807	1.11	23.4	out	--	
	III	0.805	1.10	23.2	21.0	1.05	
	IV†	0.802	1.10	23.3	22.9	1.02	
79***	I	0.809	1.19	24.9	out	--	3650
	II†	0.817	1.15	23.9	23.0	1.04	
	III	0.815	1.14	23.7	22.3	1.06	
	IV	0.808	1.12	23.5	out	--	
	V	0.809	1.11	23.3	22.5	1.04	
76	I†	0.789	1.25	26.8	out	--	3150
	II	0.798	1.21	25.7	22.5	1.14	
	III	0.787	1.20	25.8	out	--	
	IV	0.800	1.10	23.4	24.9	0.94	
80	I	0.797	1.27	27.0	24.6	1.10	3340
	II	0.799	1.26	26.7	24.2	1.10	
	III	0.789	1.23	26.4	23.5	1.12	
	IV	0.797	1.22	26.0	24.8	1.05	
	V†	0.787	1.22	26.3	No Gage	--	
77***	I†	1.010	1.19	20.1	20.5	0.98	4490
	II	1.000	1.14	19.5	18.4	1.06	
	III	1.032	1.14	18.9	19.7	0.96	
	IV	1.022	1.14	19.1	19.8	0.96	
	V	1.006	1.13	19.2	18.3	1.05	
81***	I†	1.020	1.20	20.0	18.3	1.09	4800
	II	1.010	1.16	19.6	17.5	1.12	
	III	1.040	1.15	18.9	out	--	
	IV	1.000	1.14	19.5	17.3	1.13	
	V	1.015	1.12	18.9	18.2	1.04	
78	I	0.940	1.18	21.4	out	--	4670
	II	0.991	1.18	20.3	17.8	1.14	
	III	0.930	1.17	21.4	out	--	
	IV†	0.970	1.15	20.2	out	--	
	V	0.983	1.15	20.0	17.7	1.13	
82	I	1.02	1.20	20.2	17.9	1.13	4750
	II	1.03	1.12	18.7	16.7	1.12	
	III	1.00	1.12	19.2	18.5	1.04	
	IV <sup>2</sup>	1.03	1.11	18.5	out	--	
	V	1.01	1.08	18.4	18.5	0.99	

\*The calculated stress sensitivities are determined from the equation

$$\text{Stress sensitivity} = \frac{R_{10}^2}{2 h_a R_{1m}}$$

\*\*The measured stress sensitivities are based on the average of the strain-sensitivity readings taken on the inside and outside surfaces of the shell. The strain sensitivity is defined as the slope of the portion of the pressure-strain diagram which is linear. Measured stress sensitivities are determined from the expression

$$\text{Stress sensitivity} = \frac{E}{0.2} \left[ \frac{\epsilon_1 + \epsilon_3}{1-u} + \frac{1}{1+u} \sqrt{(\epsilon_1 - \epsilon_3)^2 + [2\epsilon_2 - (\epsilon_1 + \epsilon_3)]^2} \right]$$

where  $\epsilon_1$ ,  $\epsilon_2$ , and  $\epsilon_3$  are the average strain sensitivities at the 0-, 45-, and 90-deg orientation in a three-element rosetta.

\*\*\*Stress-relieved model.

†Failure area.

stress-relieved spherical shells with initial imperfections covering the range of geometries of interest to deep submergence.

3. The effects of secondary moments and residual stresses on collapse strength diminish as the ratio of elastic to inelastic buckling pressure of the shell increases.

4. The agreement between calculated and measured membrane stresses at flat spots was fairly good. In most cases the agreement was within 10 percent, while the maximum difference was 14 percent.

#### ACKNOWLEDGMENTS

The authors wish to express their appreciation to Mr. T.J. Kiernan for his continued interest in the conduct of this project. The assistance of Mr. R.M. Charles in directing the fabrication, instrumentation, and testing of the models is also acknowledged.

#### REFERENCES

1. Krenzke, M.A., "Tests of Machined Deep Spherical Shells under External Hydrostatic Pressure," David Taylor Model Basin Report 1601 (May 1962).
2. Krenzke, M.A., "The Elastic Buckling Strength of Near-Perfect Deep Spherical Shells with Ideal Boundaries," David Taylor Model Basin Report 1713 (Jul 1963).
3. Krenzke, M.A. and Kiernan, T.J., "Tests of Stiffened and Unstiffened Machined Spherical Shells under External Hydrostatic Pressure," David Taylor Model Basin Report 1741 (Aug 1963).
4. Krenzke, M.A. and Kiernan, T.J., "Elastic Stability of Near-Perfect Shallow Spherical Shells," American Institute of Aeronautics and Astronautics Journal, Vol. 1, No. 12, p. 2857 (Dec 1963).
5. Krenzke, M.A. and Kiernan, T.J., "The Effect of Initial Imperfections on the Collapse Strength of Deep Spherical Shells," David Taylor Model Basin Report 1757 (Feb 1965).
6. Kiernan, T.J. and Nishida, K., "The Buckling Strength of Fabricated HY-80 Steel Spherical Shells," David Taylor Model Basin Report 1721 (Jul 1966).
7. Kiernan, T.J., "Predictions of the Collapse Strength of Three HY-100 Steel Spherical Hulls Fabricated for the Oceanographic Research Vehicle ALVIN," David Taylor Model Basin Report 1792 (Mar 1964).

UNCLASSIFIED

Security Classification

DOCUMENT CONTROL DATA - R & D		
<i>(Security classification of title, body of abstract and indexing annotation must be entered when the overall report is classified)</i>		
1. ORIGINATING ACTIVITY (Corporate author) Naval Ship Research and Development Center Washington, D.C. 20007		2a. REPORT SECURITY CLASSIFICATION Unclassified
		2b. GROUP
3. REPORT TITLE THE INELASTIC BUCKLING STRENGTH OF FABRICATED HY-80 STEEL HEMISPHERICAL SHELLS		
4. DESCRIPTIVE NOTES (Type of report and inclusive dates) Final Report		
5. AUTHOR(S) (First name, middle initial, last name) Costello, Malcolm G. and Nishida, Kanehiro		
6. REPORT DATE April 1967	7a. TOTAL NO. OF PAGES 45	7b. NO. OF REFS 7
8a. CONTRACT OR GRANT NO.	9a. ORIGINATOR'S REPORT NUMBER(S) 2304	
b. PROJECT NO. S-F013 01 03, Task 0214 S-F013 03 02, Task 1960		
c.	9b. OTHER REPORT NO(S) (Any other numbers that may be assigned this report)	
d.		
10. DISTRIBUTION STATEMENT Distribution of this document is unlimited.		
11. SUPPLEMENTARY NOTES		12. SPONSORING MILITARY ACTIVITY 1. Special Projects Office 2. Naval Ship Systems Command
13. ABSTRACT Eight, 66-in.-diameter, fabricated HY-80 steel hemispherical shells designed to fail by inelastic buckling were tested to observe the effects of initial imperfections and residual stresses on elastic behavior and collapse strength. The results demonstrate that the effect of secondary moments and residual stresses on collapse strength diminish as the ratio of elastic to inelastic buckling pressure increases. It was possible to predict the collapse pressures of these models within $\pm 10$ percent by utilizing imperfection analysis and extrapolating previous test results of less stable shells. Fairly good agreement was also obtained by using the same imperfection analysis to predict the membrane stresses in the center of the flat spots. Addition of the results of these tests to those obtained on shells in the less stable regions provides a basis for a reasonable collapse equation for practical spherical shells over the range of shell stability of interest to deep submergence.		

UNCLASSIFIED

Security Classification

14. KEY WORDS	LINK A		LINK B		LINK C	
	ROLE	WT	ROLE	WT	ROLE	WT
Spherical Shells Elastic Buckling Inelastic Buckling Initial Imperfections Residual Stresses Critical Local Geometry						

UNCLASSIFIED

Security Classification